Reviews in Mineralogy & Geochemistry
Vol. 72 pp. 509-557, 2010

Diffusion of Noble Gases in Minerals

Ethan F. Baxter

Department of Earth Sciences
Boston University
675 Commonwealth Ave
Boston, Massachusetts 02215, U.S.A.

efb@bu.edu

INTRODUCTION

The study of the diffusion of the six noble gas elements, helium (He), neon (Ne), argon (Ar), krypton (Kr), xenon (Xe), and radon (Rn) in minerals has spanned many decades with the primary geoscience focus on argon and helium (see below). The primary aim of this chapter is to acquaint the reader with the breadth of themes and perspectives that have accompanied the study of noble gas diffusion in minerals, and in addition, to attempt to bring the reader up to date with a focus on the most recent data and ideas from the literature of the past decade wherever possible. In this chapter, the available data for the diffusivity of each noble gas will be reviewed in turn, beginning with helium, then argon, followed by the rest of the gases. For specific minerals that have received considerably more attention than others, individual sections of this paper will be devoted to them. The data tables which accompany this chapter list the diffusion data cited herein; these tables are also available as an online supplement and from the author in excel format upon request. In general, every effort was made to compile all modern data where diffusivities have been *quantified* (i.e., where robust measurements of both activation energy and pre-exponential factor have been derived), though some early studies which have been superseded by more recent work will not be discussed. To begin, the first section describes the interpretive challenges associated with the most common method of observation for evaluation of noble gas diffusion in minerals: bulk degassing experiments. Then, following the review of the noble gas diffusion data, the remaining sections of the chapter focus on several broad themes that arise from the data that may span several noble gases or many minerals.

The applicability of noble gases and noble gas geochemistry in the geosciences may crudely be categorized into two bins: geochronology and tracer studies. Within these two categories, the use and applicability of noble gases spans a remarkable range of the earth and planetary sciences (e.g., McDougall and Harrison 1999; Ozima and Podosek 2002; Porcelli et al. 2002; Reiners and Ehlers 2005). Studies of the diffusion of noble gases in minerals have been dominated by applications in thermochronology almost entirely involving just the radionuclides producing He and Ar. Indeed, the fact that the diffusivities of uncharged He and Ar are generally much higher than cation diffusivities in minerals (with the possible exception of Li and H; e.g., see Cherniak 2010; Cherniak and Dimanov 2010; Farver 2010) makes the K-Ar and, especially, the (U-Th)/He decay systems well suited for low temperature thermochronology. Thus, there is a relative abundance of He and Ar diffusion studies in the geosciences literature in order to quantify the retentivity of radiogenic (as well as nucleogenic and cosmogenic) Ar and He as a function of mineralogy, temperature, and other intensive and extensive physical parameters. Ar and He will thus comprise the vast majority of the data and discussion presented in this chapter. While some reference to, and discussion of, thermochronology is unavoidable here, detailed discussion of the geo-thermochronologic applications and implications involving aspects of noble gas diffusion

1529-6466/10/0072-0011$05.00 DOI: 10.2138/rmg.2010.72.11

within rocks and minerals is beyond the intended context of the present chapter. For different perspectives on the role of solid-state diffusion in thermochronology, the reader is referred to a vast literature including McDougall and Harrison (1999), Kelley (2002), Farley (2002), Baxter (2003a), Reiners and Ehlers (2005), Reiners (2009), Villa (2010), Watson et al. (2010a) and references therein. After He and Ar, diffusion data for the other noble gases (Ne, Kr, Xe, Rn) is extremely scant in the published literature. Some significant work has been done to measure the diffusivities of all noble gases in melts and glasses, which is the topic of another chapter in this volume (Behrens 2010). There is a history of noble gas analyses of meteorites and other extraterrestrial objects, and in this context there have been some studies of the "bulk retentivity" of noble gases in what amount to poly-mineralic rock fragments (e.g., Burkland et al. 1995). Bulk diffusive transport studies of Rn have also been conducted on sediment and soil samples for environmental and health safety purposes. Several studies describe the bulk diffusion of Ar through rocks, outcrops, or at the scale of large crustal sections (e.g., Hyodo and York 1993; Scaillet 1996; Baxter et al. 2002; Ballentine and Burnard 2002). However, all of these bulk rock/sediment studies describe the complex integrated transport characteristics of several minerals, amorphous phases, pore fluids or gases, and grain boundaries, making extrapolations of such bulk data to other materials or systems impossible. Thus, such bulk multi-mineral (e.g., rock) diffusion reports are not included within this chapter. A final source of diffusion data on the noble gases comes from the materials science and nuclear industry literature where studies of (mostly) He mobility after implantation into metals and certain ceramics (but generally not silicates) are of great interest (and concern) in the construction and integrity of nuclear reactors or other storage vessels including nuclear waste containment (e.g., Weber and Ewing 2002). Because these materials are generally not naturally occurring (and hence not minerals in the strictest sense, cf. Dana), these reports from the materials science literature will also be mostly excluded from this chapter.

The interpretive challenge of bulk-degassing experiments

Virtually all noble gas diffusion data (with the exception of the handful of recent laser ablation, Rutherford Backscattering Analysis (RBS), and Nuclear Reaction Analysis (NRA) depth profiling studies; see references within later sections) are derived from bulk thermal release experiments conducted by heating a single crystal or a population of crystals typically sieved to a uniform grain size. This may be done by measuring the total bulk loss during isothermal heating and using simple equations for diffusive loss for an appropriate geometry to determine the diffusivities (e.g., Crank 1975). This may also be done by step-heating the specimen in vacuum and measuring the quantity of gas released during each temperature step and extracting diffusion parameters from the gas released and duration at each temperature step using the formulation of Fechtig and Kalbitzer (1966) (or a variant thereof; e.g., McDougall and Harrison 1999). Refinements in temperature calibration during step-heating experiments, for example as provided by the projector lamp apparatus of Farley et al. (1999), are crucial in yielding accurate data in this regard. In total, several bulk loss experiments conducted at different temperatures or a single step-heated bulk release experiment yields a quantification of two key parameters: E_a (the activation energy) and D_0/a^2, where D_0 is the pre-exponential factor and "a" is the diffusive lengthscale for that mineral specimen. It is important to realize that these bulk degassing experiments do not directly constrain D_0. Thus, it is for this reason that D_0/a^2 reported by most bulk degassing studies are given in many of the tables. In such cases, values of D_0 have been computed and tabulated by the present author from an assumed diffusion lengthscale (usually the reported grain size) to permit more direct and generalizable comparisons to diffusivities in other minerals. However, some unavoidable interpretive uncertainties and/or assumptions arise from this point on.

Assumption of initial diffusant distribution. The analytical formulation of Fechtig and Kalbitzer (1966) is based on the requirement of an initial spatially uniform distribution of the

diffusing species. Any significant initial intra-crystalline concentration gradients will result in skewed apparent diffusivities. Use of natural crystals that may have experienced complex growth or thermal histories and thus may have spatially heterogeneous noble gas distributions may be poor choices for diffusion experiments. To circumvent this, natural samples with simple thermal histories (e.g., rapid cooling), or cores of large crystals may be useful. Irradiated samples with uniform distribution of a parent nuclide will also produce uniform initial distributions. Shuster and Farley (2004) developed a method to evaluate and correct for heterogeneous initial ^{4}He distribution in natural samples by way of proton-irradiation produced ^{3}He.

Choice of diffusive lengthscale or domain size. In many noble gas diffusion studies, no attempt is made to identify "*a*," nor therefore to directly quantify D_0. Indeed, this is often explicitly avoided as the assignment of a unique value for "a" can be a challenge in some cases, especially for bulk multi-grain experiments. However, when general comparisons of different mineral diffusivities from different experiments are desired (such as the case in this chapter) the identification and quantification of the relevant diffusive lengthscale(s) require some further interpretation. The simplest approach is to simply take the average radial dimension of the crystal(s) in the experiment as "*a*." Here the assumption is that the macroscopic crystal dimensions control the diffusive loss and that no "fast paths" or micro "domains" exist to short circuit the macroscopic diffusion distance. If this is true, calculation of D_0 from D_0/a^2 for grains of varying size should all arrive at the same value (within experimental and analytical uncertainty). In some studies, this has been argued to be the case (Foland 1974; Farley 2000; Reiners et al. 2004; Cassata et al. 2009) and the macroscopic grain size is the diffusion lengthscale. However, in others the apparent D_0 derived from grains of different size varies significantly, and/or Arrhenian relationships from degassing experiments are complex, suggesting that the macroscopic crystal is not the relevant diffusive lengthscale (e.g., Harrison et al. 1985; Lovera et al. 1989, 1997; Wolf et al. 1996; Copeland et al. 2007; Harrison et al. 2009). In these studies, the interpretation is instead that there are small domains within the crystal surrounded by fast pathways that control the diffusive loss. It is also possible, despite efforts to sieve samples to a relatively uniform grain size distribution, that a small but measureable fraction of a bulk sample can consist of significantly differently sized grains that will complicate the bulk release characteristics (e.g., Harrison et al. 2009). Still other studies have argued that bulk release experiments yielding complex Arrhenian behavior reflect the operation of complex processes that may have little to do with simple Fickian diffusion (e.g., Villa 2010).

Geometry and anisotropy of diffusion. Interpretations of bulk release data require an assumption not just of the appropriate diffusion geometry (sphere, cylinder, plane, etc.), but also the extent of anisotropy in diffusion, which can be significant in some minerals. The Fechtig and Kalbitzer (1966) approach requires the simplifying assumption that diffusion is isotropic with spherical geometry. This results in an averaging effect, producing diffusion parameters that might be a convolution of more complex geometries and diffusional anisotropy. Fortunately, according to new modeling by (Watson et al. 2010b), the bulk isotropic spherical approximation will generally produce diffusion parameters that track the *least* retentive (i.e., fastest) diffusion direction and thus the effect on natural applications (such as closure temperatures) will be small.

Interpretation of non-Arrhenian (i.e., non-linear) behavior. The uncertainty in the effective diffusion lengthscale underscores the broader interpretive assumption inherent in all noble gas bulk thermal release studies: the assumption that release is controlled by Fickian diffusion within a homogeneous and stable mineral structure. Perhaps this issue with bulk release studies is belied best by the words used in many titles of such papers. Rather than "diffusion," paper titles often describe "release" or "degassing" characteristics of noble gases from minerals. While the term "diffusion" has perhaps been known to connote any molecular or atomic scale migration process, *sensu strictu* the word connotes something much more specific

in terms of the physical mechanisms and mathematical formalisms used to describe it. Fickian diffusion (obeying Fick's laws; Fick 1855; Crank 1975) would be characterized by a linear (Arrhenian; i.e., linear in log$D$ vs. $1/T$) thermal release pattern indicative of a single diffusive transport mechanism operating in a homogeneous and non-evolving medium. Villa (2010) suggests that bulk degassing studies necessarily reflect a combination of possible release mechanisms—which may well include Fickian diffusion, but also include the contributions of fast paths, structural breakdown, or dissolution—such that deconvolving the bulk release signal into an easily extrapolatable set of Arrhenian diffusion parameters is challenging (at best) and "futile" (at worst). Even a cursory look at available thermal release data for noble gases from minerals shows that simple linear Arrhenian behavior is quite often not evident (Fig. 1). For example, helium in apatite data show a decreased slope in the Arrhenius relation to lower apparent activation energies at higher temperatures (above ~265 °C; e.g., Farley 2000) and He in titanite shows a flattening at low temperatures. Hetherington and Villa (2007) show bulk release data for Ar and Xe from several silicates some of which display non-Arrhenian behavior. These and other authors offer various explanations for these deviations from linearity, but the point is that Arrhenian diffusion seems actually quite the exception rather than the rule in noble gas bulk release experiments. However, it is often the case that over a large temperature span a linear relationship is evident that may judiciously be extrapolated, permitting us to ignore data which may deviate from the linear Arrhenius relation at different temperatures. For the thermochronologic applications, this approach seems to be adequate; however from the standpoint of understanding the

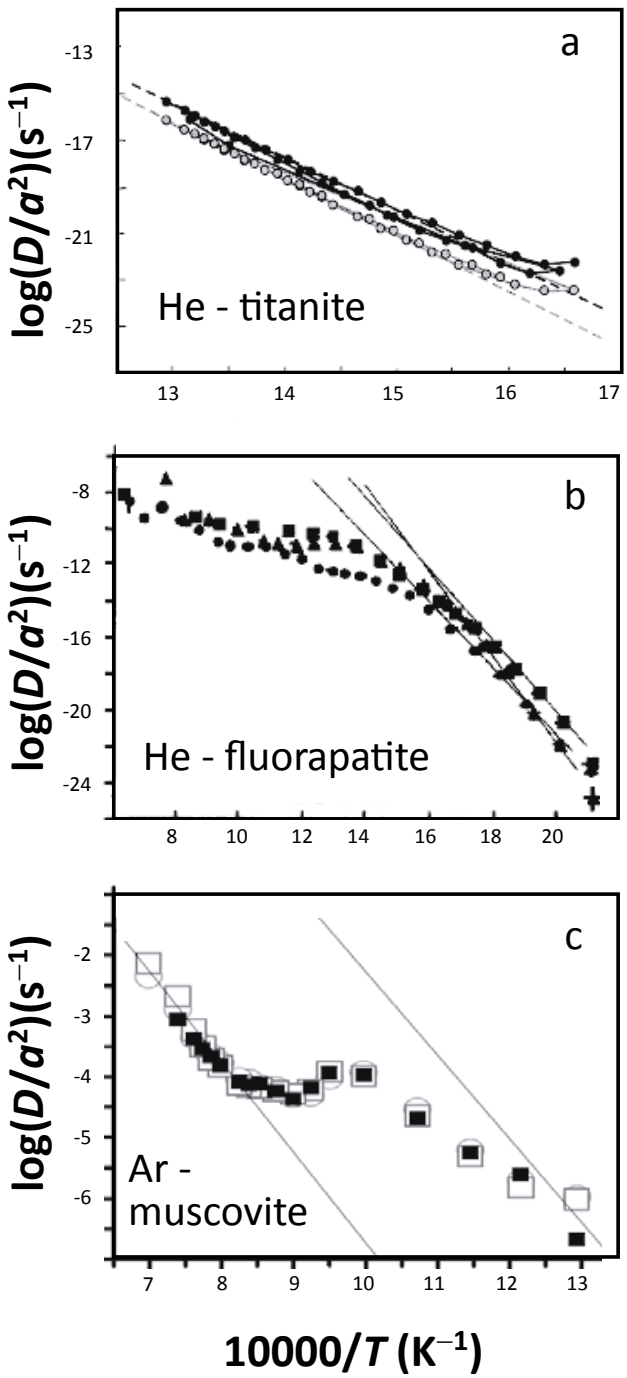

Figure 1. Arrhemius plots showing examples of deviations from linear diffusion behavior. a) He in titanite (Reiners and Farley 1999), b) He in apatite (Warnock et al. 1997), c) Ar in muscovite (Harrison et al. 2009). Many other examples exist (see text). Modified figures used by permission of Elsevier Ltd., from Reiners and Farley (1999), Geochimica et Cosmochimica Acta, Vol. 63, Fig. 1, p. 3846; Warnock et al. (1997) Geochimica et Cosmochimica Acta, Vol. 61, Fig. 3, p. 5376; Harrison et al. (2009) Geochimica et Cosmochimica Acta, Vol. 73, Fig. 9, p. 1045.

phenomenology of diffusion of the noble gases in these minerals, it is somewhat unsatisfying. At worst, bulk release data produce a constraint on the actual diffusivity of noble gases—the net bulk release behavior would represent a maximum value for the lattice diffusivity. Most likely, in order for significant progress to be made in deciphering the specific physical mechanisms behind deviations from pure Arrhenian behavior, a specific scientific application requiring (and/or unearthing) such knowledge would need to arise. Two good examples merit introduction in this context: Ar in potassium feldspar, and He in apatite. In the case of K-feldspar, its great potential for thermochronology led to the develoopment of the "Multi-diffusion domain" (MDD) model (e.g., Lovera et al. 1989, 1997) which has been used to interpret complex thermal release patterns in terms of detailed natural thermal histories. Its development also led to subsequent controversy and sparked new research (see below). Consensus on the release mechanisms and diffusivity of Ar in potassium feldspar has not been reached, but vigorous debate and scientific inquiry has made this one of the best studied minerals for noble gas diffusivity. For the case of He in apatite, its use as a low-temperature thermochronometer bringing together tectonics and surface processes drove unprecedented technique development and data on diffusion, including recent work to quantify the distribution of He within apatites to aid in thermochronologic interpretations (Shuster and Farley 2004), as well as to evaluate the role of radiation damage in altering He diffusivity over time (e.g., Shuster and Farley 2009). Advances in our understanding of the processes that affect the bulk diffusive release of noble gases from minerals in nature have been generated from this significant body of bulk release studies, precisely by recognizing and addressing the inherent uncertainties and complexities.

The next sections of this chapter summarize and illuminate modern approaches and constraints on the diffusion (or bulk release characteristics) of noble gases from minerals, including where recent breakthroughs and controversies exist.

HELIUM

Interest in the diffusive loss of helium from minerals probably goes back to the very first attempts at geochronology (e.g., Strutt 1908; Damon and Kulp 1957) where U-He ages were found to be unreasonably young due to leakage from these old minerals. Then, based on early reports of excess ^{4}He in cyclosilicates (e.g., beryl, cordierite; see Rayleigh 1933 and Damon and Kulp 1957) some studies in diffusion were devoted to understanding the possible origins of this helium (e.g., Toyota and Ozima 1988). Once it was deemed that helium would not be a particularly fruitful avenue for robust geochronological research, interests in helium diffusivity in minerals instead moved into its behavior as a tracer of mantle evolution and planetary degassing (e.g., olivine: Hart 1984, Trull and Kurz 1993; diamond: Honda et al. 1987, Ozima 1989, Zashu and Hiyagon 1995, Weins et al. 1994; pyroxene: Trull and Kurz 1993), cycling of "solar" helium within IDPs into the mantle (Hiyagon 1994), and cosmogenic surface exposure age dating (quartz, olivine: Trull et al. 1991; Shuster et al. 2004; Shuster and Farley 2005). The major resurgence of helium diffusion studies came with the recognition that the leakiness of helium, if appropriately quantified, could be used to advantage in the form of a very low-temperature thermochronometer (Zeitler et al. 1987; Lippolt and Weigel 1988). Diffusion studies by Lippolt and co-workers (Lippolt and Weigel 1988; Bahr et al. 1994) explored the diffusivity of helium in a great many minerals (augite, hematite, hornblende, langbeinite, muscovite, nephelilne, sanidine). But starting with the contribution by Wolf et al. (1996), the vast majority of modern helium diffusion measurements have been conducted in U and Th rich minerals well suited to low-temperature thermochronology, primarily apatite as well as zircon, titanite, monazite, and even calcite (Copeland et al. 2007) and goethite (Shuster et al. 2005).

Measurement of helium diffusivity has been almost exclusively via step heating release experiments on single grains or on multi-grain fractions. In most cases, the bulk thermal release pattern can be used to extract Arrhenius diffusion parameters using the formulation of Fechtig

and Kalbitzer (1966). The only exceptions include, 1) recent work by Cherniak et al. (2009) and Cherniak and Watson (2009) who use Nuclear Reaction Analysis to directly measure diffusive broadening profiles of implanted ^{3}He in apatite, zircon, monazite and titanite, 2) work by Parman et al. (2009) who have developed a laser depth profiling technique capable of measuring diffusive uptake profiles of ^{4}He in olivine, and 3) work by Ouchani et al. (1998) who measured diffusion of helium in Durango fluorapatite using elastic recoil detection (ERD). The work of Toyota and Ozima (1988) and Boyce et al. (2005) also employed a laser extraction method to isolate small spatial domains within single crystals, but still relied on step heating experiments to derive diffusion parameters.

He in apatite

Due to its frequent use as a low-temperature thermochronometer, apatite is by far the mineral most widely studied for helium diffusion. Since 1987, ten experimental studies of helium diffusion in apatite have been published in the geosciences literature. All except two (Ouchani et al. 1998 and Cherniak et al. 2009 who use ERD and NRA methods respectively; see above) employ bulk step heating analyses of helium loss from apatite, often on single grains or cut wafers. *In situ* NRA methods as well as elastic recoil detection (ERD) methods have been used to provide constraints on helium diffusion in synthetic apatite ceramics in the context of nuclear industrial applications (e.g., see Cherniak et al. 2009 for a review of these studies).

The available data provide an opportunity to cross-check and compare bulk-release and direct profiling results. Table 1 and Figure 2 show diffusion results for helium in apatite. With the exception of a few spurious results, these findings are similar. On the basis of a large dataset of repeat bulk step heating diffusion experiments on the well-characterized Durango apatite, Farley (2000) provides a "best estimate" of E_a = 138±2 kJ/mol and $\log D_0$ = –2.5±0.6 m^2/s. Comparison of the study by Farley (2000) (which provides a robust step-release result) and the Cherniak et al. (2009) result from direct NRA profiling (both studies use the Durango apatite) shows that the two yield broadly similar activation energies for He diffusion (138±2 kJ/mol for ^{4}He in Farley 2000; 127±12 and 117±6 for ^{3}He in Cherniak et al. 2009), though the diffusivities differ by about one order of magnitude over the range of experimental temperatures. Part of the apparent difference in activation energy could be due to the fact that Farley (2000) (as well as other bulk-release studies; i.e., Zeitler et al. 1987; Wolf et al. 1996; Warnock et al. 1997; Shuster et al. 2004) observed a marked decrease in slope of the Arrhenius relationship toward lower activation energies at higher temperatures (above ~265 °C) and consequently did not include those data in his regression, leading to slightly higher overall activation energy. Warnock et al. (1997) further suggest that there may be a compositional (mainly related to Cl content) dependence on the temperature at which this "roll-over" point from higher to lower activation energy occurs in natural apatites. Interestingly, Cherniak et al. (2009) did not observe any departure from linear Arrhenian behavior at high temperatures. The order of magnitude difference in diffusivity between the bulk-release (higher) and NRA (lower) studies of Durango apatite could perhaps be partially ascribed to the uncertainty and approximations in the diffusion lengthscale and geometry of the bulk release experiments of Farley (2000) as they involved crushed and sieved multi-grain samples with spherical geometry assumed. With sieved grain size varying up to 50% in the Farley (2000) study, the a^2 dependence on bulk diffusion could lead to an offset of about a factor of two. Cylindrical (or planar) diffusion geometry, which may more closely approximate elongated or flattened "shards" of crushed and splintered apatite, could lead to an offset of an additional factor of 2 or more. Additionally, Boyce and Hodges (2005) discussed the possible effects of compositional heterogeneity (i.e., distribution of helium-generating parent elements such as U and Th) in the calculation of bulk grain (U-Th)/He apatite ages and caution that the use of small grain fragments could lead to inconsistent apparent bulk release behavior. Shuster and Farley (2004) developed the ^{4}He/^{3}He thermochronometer method to address and account for such spatial heterogeneities in U-Th produced ^{4}He. Overall, the fact

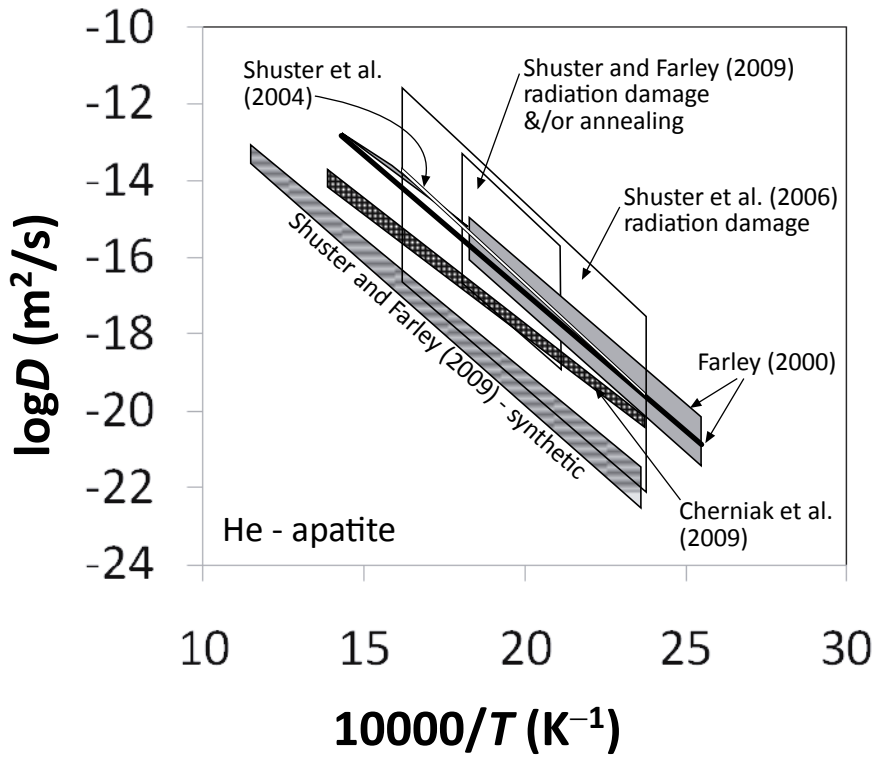

Figure 2. Diffusion data for helium in apatite since 2000. Each field represents the full span of all linear Arrhenius relationships derived from the multiple experiments of each study (see Table 1). Gray - Farley (2000) step-heating analysis of Durango apatite. Black line - "Best estimate" from Farley (2000). Narrow white - Shuster et al. (2004) step heat analysis of Durango apatite. Stippled - Cherniak et al. (2009) NRA analysis of Durango apatite. Striped - Shuster and Farley (2009) step heat analysis of synthetic fluorapatite. Open - Shuster et al. (2006) and Shuster and Farley (2009) step heating analysis of irradiated and/or annealed apatites (including Durango and many natural apatites). Radiation damage and annealing can significantly alter the diffusivity of helium in apatite.

that the activation energies are in good agreement and that the absolute diffusivities are within an order of magnitude (despite grain size geometry uncertainties) is strong validation of each of these two methods of observation for He in apatite, and of the diffusive behavior in general. Cherniak et al. (2009) and Farley (2000) also both explore diffusional anisotropy in apatite by sectioning slabs parallel and perpendicular to the *c*-axis. Both studies conclude that there is no significant anisotropy in apatite. Farley (2000) also explored the effects of varying grain size, concluding that the macroscopic grain dimension was the relevant diffusion dimension (at least for the range of grain sizes studied; 44-180 μm), in contrast to earlier work by Wolf et al. (1996) who employed less advanced analytical methods.

Shuster et al. (2004) studied both naturally occurring ^{4}He and ^{3}He diffusion in Durango apatite by means of doping the mineral with ^{3}He via spallation reactions in response to proton bombardment. Their results show that ^{3}He and ^{4}He diffuse at the same rate. This result is contrary to the square-root-of-mass dependence that would be predicted from molecular kinetic models, suggesting that such models are not valid for helium in apatite (and perhaps not for diffusion in most solids). Rather, Shuster et al. (2004) suggest that the mass independence of He diffusion may be due to the dominant role of defects in the crystal structure in accommodating the diffusive migration. The important controlling role of defects—including structural defects that may result from progressive radiation damage—was further explored in several papers by Shuster and co-workers. These radiation damage effects are discussed separately in a later section.

Table 1. Diffusion of helium in apatite.

Apatite sample	Species	Orientation	T(K)	E_a (kJ/mol)	±	D_0 (m^2/s)	log D_0[†]	±	log D_0/a^2	a (μm)	Notes	Reference
Durango	^{3}He	*c*-perp	421-722	117	6	2.10E-06	−5.68	0.60	na	na	c,e,f	Cherniak et al. (2009)
Durango	^{3}He	*c*-para	421-722	129	12	4.21E-05	−4.38	1.14	na	na	c,e,f	Cherniak et al. (2009)
Durango	^{4}He	bulk	473-553	141	1.7	1.09E-02	−1.96	0.17	6.18	85	a	Shuster and Farley (2009)
Durango	^{4}He	bulk	473-553	140	2.5	1.07E-02	−1.97	0.26	6.17	85	a,g	Shuster and Farley (2009)
Durango	^{4}He	bulk	473-553	137	1.7	3.13E-03	−2.50	0.17	5.64	85	a,g	Shuster and Farley (2009)
Durango	^{4}He	bulk	473-553	133	1.6	2.89E-03	−2.54	0.17	5.60	85	a,g	Shuster and Farley (2009)
Durango	^{4}He	bulk	473-553	127	1.5	3.37E-04	−3.47	0.16	4.67	85	a,g	Shuster and Farley (2009)
Durango	^{4}He	bulk	473-553	123	2.3	1.89E-04	−3.72	0.24	4.42	85	a,g	Shuster and Farley (2009)
Durango	^{4}He	bulk	473-553	121	1.2	6.15E-05	−4.21	0.17	3.93	85	a,g	Shuster and Farley (2009)
Durango	^{4}He	bulk	473-553	117	1.5	3.70E-05	−4.43	0.15	3.71	85	a,g	Shuster and Farley (2009)
Durango	^{4}He	bulk	473-553	112	1.9	9.77E-06	−5.01	0.20	3.13	85	a,g	Shuster and Farley (2009)
Durango	^{4}He	bulk	473-553	108	1.3	6.36E-06	−5.20	0.14	2.94	85	a,g	Shuster and Farley (2009)
Durango	^{4}He	bulk	473-553	94	1.3	6.98E-07	−6.16	0.14	1.98	85	a,g	Shuster and Farley (2009)
Durango	^{4}He	bulk	473-553	79	1.3	1.19E-08	−7.92	0.14	0.22	85	a,g	Shuster and Farley (2009)
Durango	^{4}He	bulk	473-553	142	1.7	8.43E-03	−2.07	0.18	6.07	85	a,g	Shuster and Farley (2009)
Durango	^{4}He	bulk	473-553	135	1.7	2.30E-03	−2.64	0.17	5.50	85	a,g	Shuster and Farley (2009)
Durango	^{4}He	bulk	473-553	125	2	3.61E-04	−3.44	0.16	4.70	85	a,g	Shuster and Farley (2009)
Durango	^{4}He	bulk	473-553	125	1.5	2.40E-04	−3.62	0.16	4.52	85	a,g	Shuster and Farley (2009)
Durango	^{4}He	bulk	473-553	119	1.5	4.17E-05	−4.38	0.15	3.76	85	a,g	Shuster and Farley (2009)
Durango	^{4}He	bulk	473-553	109	1.3	3.42E-06	−5.47	0.14	2.67	85	a,g	Shuster and Farley (2009)
Durango	^{4}He	bulk	473-553	135	1.7	1.64E-03	−2.79	0.17	5.35	85	a,g	Shuster and Farley (2009)
Durango	^{4}He	bulk	473-553	129	1.6	6.14E-04	−3.21	0.17	4.93	85	a,g	Shuster and Farley (2009)
Durango	^{4}He	bulk	473-553	118	1.5	1.12E-05	−4.95	0.15	3.19	85	a,g	Shuster and Farley (2009)
Durango	^{4}He	bulk	473-553	118	1.9	1.06E-05	−4.98	0.20	3.17	85	a,g	Shuster and Farley (2009)
Durango	^{4}He	bulk	473-553	133	1.8	1.48E-03	−2.83	0.19	5.31	85	a,g	Shuster and Farley (2009)
Durango	^{4}He	bulk	473-553	126	1.7	1.48E-04	−3.83	0.18	4.31	85	a,g	Shuster and Farley (2009)
Durango	^{4}He	bulk	473-554	141	2.7	8.69E-03	−2.06	0.26	6.08	85	a	Shuster and Farley (2009)
Durango	^{4}He	bulk	473-555	145	3.5	8.16E-02	−1.09	0.37	7.05	85	a,g	Shuster and Farley (2009)
Durango	^{4}He	bulk	473-556	143	2	1.82E-02	−1.74	0.20	6.40	85	a,g	Shuster and Farley (2009)
Durango	^{4}He	bulk	473-557	135	1.9	2.62E-03	−2.58	0.20	5.56	85	a,g	Shuster and Farley (2009)
Durango	^{4}He	bulk	473-558	133	1.6	2.25E-03	−2.65	0.17	5.49	85	a,g	Shuster and Farley (2009)
Durango	^{4}He	bulk	473-559	127	1.5	1.05E-03	−2.98	0.16	5.16	85	a,g	Shuster and Farley (2009)
Durango	^{4}He	bulk	473-560	115	1.4	1.54E-04	−3.81	0.14	4.33	85	a,g	Shuster and Farley (2009)

(Table 1 continued on next page)

Apatite sample	Species	Orientation	T(K)	E_a (kJ/mol)	±	D_0 (m^2/s)	log D_0†	±	log D_0/a^2	a (μm)	Notes	Reference
Durango	^{4}He	bulk	473-561	115	1.4	1.04E-04	−3.98	0.14	4.16	85	a,g	Shuster and Farley (2009)
fluorapatite synth.	^{3}He	bulk	423-873	132	0.8	6.46E-06	−5.19	0.06	2.46	150	a,d	Shuster and Farley (2009)
fluorapatite synth.	^{3}He	bulk	423-873	133	1.1	7.58E-06	−5.12	0.09	2.53	150	a,d,h	Shuster and Farley (2009)
fluorapatite synth.	^{3}He	bulk	423-873	132	1.8	2.65E-06	−5.58	0.14	2.07	150	a,d,h	Shuster and Farley (2009)
fluorapatite synth.	^{3}He	bulk	423-873	149	0.6	6.98E-05	−4.16	0.04	3.49	150	a,d,h	Shuster and Farley (2009)
00mr18_A	^{3}He	bulk	473-553	165	4.7	4.43E+00	0.65	0.52	9.18	54	a,d,h	Shuster and Farley (2009)
00mr18b	^{3}He	bulk	473-553	149	2.7	5.68E+00	0.75	0.30	9.29	54	a,d	Shuster and Farley (2009)
01mr59_A	^{3}He	bulk	473-553	123	1.2	3.59E-04	−3.44	0.13	5.09	54	a,d,h	Shuster and Farley (2009)
01mr59_B	^{3}He	bulk	473-553	134	2.1	3.00E-04	−3.52	0.23	5.02	54	a,d,h	Shuster and Farley (2009)
01mr59_C	^{3}He	bulk	473-553	135	1	1.04E-03	−2.98	0.11	5.55	54	a,d,h	Shuster and Farley (2009)
01mr59a	^{3}He	bulk	473-553	121	1.5	1.05E-04	−3.98	0.17	4.56	54	a,d	Shuster and Farley (2009)
CJ50_A	^{3}He	bulk	473-553	136	0.8	1.50E-04	−3.82	0.07	4.72	54	a,d,h	Shuster and Farley (2009)
CJ50b	^{3}He	bulk	473-553	121	0.9	7.77E-05	−4.11	0.09	4.43	54	a,d	Shuster and Farley (2009)
DAp_A	^{3}He	bulk	473-553	139	2.2	2.19E-03	−2.66	0.24	5.88	54	a,d	Shuster and Farley (2009)
DAp_B	^{3}He	bulk	473-553	138	0.9	1.87E-03	−2.73	0.09	5.81	54	a,d,h	Shuster and Farley (2009)
DAp_C	^{3}He	bulk	473-553	161	2	6.62E-01	−0.18	0.22	8.36	54	a,d,h	Shuster and Farley (2009)
DAp_D	^{3}He	bulk	473-553	164	2.1	1.29E+00	0.11	0.22	8.65	54	a,d,h	Shuster and Farley (2009)
DYJS5_A	^{3}He	bulk	473-553	128	2.1	8.76E-05	−4.06	0.23	4.48	54	a,d,h	Shuster and Farley (2009)
DYJS5b	^{3}He	bulk	473-553	122	1.2	1.05E-04	−3.98	0.13	4.56	54	a,d	Shuster and Farley (2009)
Durango	^{3}He	bulk	423-623	147.9	0.7	6.60E-02	−1.18	0.07	6.96	85	a,d	Shuster et al. (2004)
Durango	^{4}He	bulk	423-623	147.7	0.5	5.30E-02	−1.28	0.05	6.87	85	a	Shuster et al. (2004)
Bolivia	^{3}He	bulk	423-623	125.9	1.3	1.18E-04	−3.93	0.13	4.52	60	a,d	Shuster et al. (2006)
Cajon Pass, CA	^{3}He	bulk	423-623	122.3	2.9	2.38E-04	−3.62	0.26	4.82	60	a,d	Shuster et al. (2006)
Cajon Pass, CA	^{3}He	bulk	423-623	120.5	0.9	9.69E-05	−4.01	0.09	4.43	60	a,d	Shuster et al. (2006)
Cajon Pass, CA	^{3}He	bulk	423-623	140.2	10	3.54E-03	−2.45	1.00	5.99	60	a,d	Shuster et al. (2006)
Cent. Coast Mtns, CAN	^{3}He	bulk	423-623	129.4	1.8	3.22E-04	−3.49	0.17	4.95	60	a,d	Shuster et al. (2006)
Cent. Coast Mtns, CAN	^{3}He	bulk	423-623	133.1	2.3	1.07E-03	−2.97	0.22	5.47	60	a,d	Shuster et al. (2006)
San Bernardino Mtns, CA	^{3}He	bulk	423-623	121.5	1.2	1.31E-04	−3.88	0.13	4.56	60	a,d	Shuster et al. (2006)
Sierra Nevada , CA	^{3}He	bulk	423-623	126.2	4	1.44E-04	−3.84	0.39	4.60	60	a,d	Shuster et al. (2006)
Sierra Nevada , CA	^{3}He	bulk	423-623	136.4	1.9	1.94E-02	−1.71	0.22	6.73	60	a,d	Shuster et al. (2006)
Sierra Nevada , CA	^{3}He	bulk	423-623	129.5	3.8	5.86E-04	−3.23	0.39	5.21	60	a,d	Shuster et al. (2006)
Sierra Nevada , CA	^{3}He	bulk	423-623	130.7	3.6	7.16E-04	−3.15	0.35	5.30	60	a,d	Shuster et al. (2006)
Sierra Nevada , CA	^{3}He	bulk	423-623	136.4	2	2.63E-03	−2.58	0.22	5.86	60	a,d	Shuster et al. (2006)
Sierra Nevada , CA	^{3}He	bulk	423-623	133.3	1.3	7.16E-04	−3.15	0.13	5.30	60	a,d	Shuster et al. (2006)

(Table 1 continued on next page)

Apatite sample	Species	Orientation	T(K)	E_a (kJ/mol)	±	D_0 (m^2/s)	log D_0[†]	±	log D_0/a^2	a (μm)	Notes	Reference
Sierra Nevada , CA	^{3}He	bulk	423-623	134.0	3.4	6.48E-04	−3.19	0.35	5.25	60	a,d	Shuster et al. (2006)
Sierra Nevada , CA	^{3}He	bulk	423-623	129.6	2.1	1.18E-04	−3.93	0.22	4.52	60	a,d	Shuster et al. (2006)
Sierra Nevada , CA	^{3}He	bulk	423-623	134.1	1.1	5.86E-04	−3.23	0.13	5.21	60	a,d	Shuster et al. (2006)
Sierra Nevada , CA	^{3}He	bulk	423-623	133.9	1.8	4.34E-04	−3.36	0.17	5.08	60	a,d	Shuster et al. (2006)
Sierra Nevada , CA	^{3}He	bulk	423-623	142.4	3.3	3.21E-03	−2.49	0.35	5.95	60	a,d	Shuster et al. (2006)
Southern Coast Mtns	^{3}He	bulk	423-623	148.9	2.7	7.08E+00	0.85	0.30	9.29	60	a,d	Shuster et al. (2006)
Southern Coast Mtns	^{3}He	bulk	423-623	121.2	1.5	1.31E-04	−3.88	0.17	4.56	60	a,d	Shuster et al. (2006)
Southern Coast Mtns	^{3}He	bulk	423-623	124.0	1	1.60E-04	−3.80	0.09	4.65	60	a,d	Shuster et al. (2006)
Southern Coast Mtns	^{3}He	bulk	423-623	123.2	1	9.69E-05	−4.01	0.13	4.43	60	a,d	Shuster et al. (2006)
Southern Coast Mtns	^{3}He	bulk	423-623	130.9	3	6.48E-04	−3.19	0.30	5.25	60	a,d	Shuster et al. (2006)
Tibet	^{3}He	bulk	423-623	119.5	2	9.69E-05	−4.01	0.22	4.43	60	a,d	Shuster et al. (2006)
Tibet	^{3}He	bulk	423-623	125.4	1.6	1.95E-04	−3.71	0.17	4.73	60	a,d	Shuster et al. (2006)
Tibet	^{3}He	bulk	423-623	127.7	1.6	3.22E-04	−3.49	0.26	4.95	60	a,d	Shuster et al. (2006)
Appalachians, PA	^{4}He	bulk	423-623	136.4	2.1	3.93E-04	−3.41	0.22	5.04	60	a	Shuster et al. (2006)
Australia	^{4}He	bulk	423-623	140.6	3.8	1.77E-05	−4.75	0.39	3.69	60	a	Shuster et al. (2006)
Big Horn Mtns, WY	^{4}He	bulk	423-623	125.1	3.8	1.07E-05	−4.97	0.39	3.47	60	a	Shuster et al. (2006)
Cent. Coast Mtns, CAN	^{4}He	bulk	423-623	109.2	0.8	2.65E-06	−5.58	0.09	2.87	60	a	Shuster et al. (2006)
Cent. Coast Mtns, CAN	^{4}He	bulk	423-623	125.4	2.1	4.81E-05	−4.32	0.22	4.13	60	a	Shuster et al. (2006)
Cent. Coast Mtns, CAN	^{4}He	bulk	423-623	126.4	1.8	6.49E-05	−4.19	0.22	4.26	60	a	Shuster et al. (2006)
Cent. Coast Mtns, CAN	^{4}He	bulk	423-623	129.3	0.7	1.31E-04	−3.88	0.09	4.56	60	a	Shuster et al. (2006)
Dry Valleys, Antarctica	^{4}He	bulk	423-623	138.1	1.3	3.92E-03	−2.41	0.13	6.04	60	a	Shuster et al. (2006)
Mexico	^{4}He	bulk	423-623	139.7	0.5	4.33E-03	−2.36	0.04	6.08	60	a	Shuster et al. (2006)
San Bernardino Mtns, CA	^{4}He	bulk	423-623	123	0.6	1.96E-05	−4.71	0.09	3.73	60	a	Shuster et al. (2006)
San Gabriel Mtns, CA	^{4}He	bulk	423-623	132.4	0.8	7.91E-04	−3.10	0.09	5.34	60	a	Shuster et al. (2006)
Snowbird, Canada	^{4}He	bulk	423-623	139.7	1.3	3.94E-05	−4.40	0.13	4.04	60	a	Shuster et al. (2006)
Snowbird, Canada	^{4}He	bulk	423-623	158.6	1.7	7.14E-03	−2.15	0.17	6.30	60	a	Shuster et al. (2006)
Wind River Mtns, WY	^{4}He	bulk	423-623	138.9	1.3	3.55E-04	−3.45	0.17	4.99	60	a	Shuster et al. (2006)
Durango	^{4}He	na	393-698	138	2	3.16E-03	−2.50	0.6	na	na	a	Farley (2000)
Durango	^{4}He	*c*-perp	393-548	137	1	3.35E-03	−1.89	0.01	5.78	75	a	Farley (2000)
Durango	^{4}He	*c*-para	393-548	128	1	1.94E-04	−3.11	0.02	4.53	75	a	Farley (2000)
Durango	^{4}He	bulk	393-548	138	1	4.94E-03	−2.31	0.07	5.83	85	a	Farley (2000)
Durango	^{4}He	bulk	393-548	138	2	4.75E-03	−2.32	0.03	6.09	62	a	Farley (2000)
Durango	^{4}He	bulk	393-548	153	4	1.45E-01	−0.84	0.04	7.89	43	a	Farley (2000)
Durango	^{4}He	bulk	393-548	148	3	5.30E-02	−1.28	0.03	7.67	34	a	Farley (2000)
Durango	^{4}He	bulk	393-548	154	4	3.40E-01	−0.47	0.04	8.75	24	a	Farley (2000)

(Table 1 continued on next page)

Apatite sample	Species	Orientation	T(K)	E_a (kJ/mol)	±	D_0 (m^2/s)	log D_0†	±	log D_0/a^2	a (μm)	Notes	Reference
Durango	^{4}He	bulk	628-493	124.7	1	5.67E-04	−3.25	0.02	4.89	85	a	Farley (2000)
Durango	^{4}He	bulk	698-493	118.5	2	1.25E-04	−3.90	0.05	4.24	85	a	Farley (2000)
Durango	^{4}He	bulk	633-433	122.2	2	3.39E-04	−3.47	0.09	4.67	85	a	Farley (2000)
chlorapatite	^{4}He	bulk	473-723	123	14	1.71E-04	−3.77	na	4.42	81	b	Warnock et al. (1997)
fluorapatite	^{4}He	bulk	473-573	167	18	1.25E+00	0.10	na	8.69	51	b	Warnock et al. (1997)
fluorapatite	^{4}He	bulk	473-573	198	10	1.28E+03	3.11	na	11.3	83	b	Warnock et al. (1997)
fluorapatite, plutonic	^{4}He	bulk	473-573	149	10	1.44E-02	−1.84	na	6.27	88	b	Warnock et al. (1997)
hydroxyapatite	^{4}He	bulk	473-573	126	13	6.81E-04	−3.17	na	5.02	81	b	Warnock et al. (1997)
Durango	^{4}He	bulk	353-524	152	4	3.62E-01	−0.44	0.5	7.7	85	b	Wolf et al. (1996)
plutonic	^{4}He	bulk	433-623	123	12	1.91E-05	−4.72	0.5	3.8	55	b	Wolf et al. (1996)
plutonic	^{4}He	bulk	443-523	151	21	4.79E-02	−1.32	2.2	7.2	55	b	Wolf et al. (1996)
plutonic	^{4}He	bulk	361-553	149	7	1.52E-01	−0.82	0.8	7.7	55	b	Wolf et al. (1996)
plutonic	^{4}He	bulk	356-544	162	5	8.30E+00	0.92	0.6	9.4	58	b	Wolf et al. (1996)
plutonic	^{4}He	bulk	415-587	146	8	2.85E-03	−2.55	0.8	6.5	30	b	Wolf et al. (1996)
hydrothermal	^{4}He	bulk	473-773	196	11	6.31E+01	1.80	1	na	na	b	Lippolt et al. (1994)
hydrothermal	^{4}He	bulk	473-773	156	6	9.33E-05	−4.03	0.56	na	na	b	Lippolt et al. (1994)
hydrothermal	^{4}He	bulk	473-773	73	3	2.51E-09	−8.60	0.3	na	na	b	Lippolt et al. (1994)
hydrothermal	^{4}He	bulk	473-773	65	3	6.31E-11	−10.20	0.8	na	na	b	Lippolt et al. (1994)
plutonic	^{4}He	bulk	473-773	142	3	6.31E-04	−3.20	0.45	na	na	b	Lippolt et al. (1994)
plutonic	^{4}He	bulk	473-773	146	5	1.00E-03	−3.00	0.5	na	na	b	Lippolt et al. (1994)
pneumatolytic	^{4}He	bulk	473-773	116	3	3.16E-05	−4.50	1.2	na	na	b	Lippolt et al. (1994)
pneumatolytic	^{4}He	bulk	473-773	99	4	3.16E-07	−6.50	0.65	na	na	b	Lippolt et al. (1994)
Durango	^{4}He	bulk	523-673	161	17	9.02E-02	−1.04	0.6	7.12	83	b	Zeitler et al. (1987)

all diffusivities for vaccuum pressures, except as noted; all uncertainties given at 1σ.

†Many studies give only D_0/a^2; in these cases D_0 is calculated from D_0/a^2 and reported grain size "a" as indicated.

Notes: a - projector lamp step heating and mass spectrometric analysis; b - resistance furnace step heating and mass spectrometric analysis; c - nuclear reaction analysis depth profiling; d - proton bombardment produced ^{3}He; e - implanted helium; f - 1 atm furnace degassing experiment; g - annealed; h - neutron irraditation induced damage

He in titanite

Reiners and Farley (1999), Shuster et al. (2004), and Cherniak and Watson (2009) all explore diffusion of He in titanite (Table 2 and Fig. 3). The former two studies employ step-heating release experiments while the latter uses NRA. As in the case of apatite, the two different analytical methodologies give comparable results. Also like apatite, bulk release experiments on titanite show deviations from linearity of the Arrhenius relationship, only in this case at the lowest temperatures. Shuster et al. (2004) shows that the lower temperature relationship (with lower activation energy) accounts for only ~1% of the total helium released. Also, given that ^{3}He and ^{4}He release characteristics are decoupled in this low temperature array, Shuster et al. (2004) suggest that some or all of the natural ^{4}He that might have existed within these low-retentivity "domains" may have diffused out prior to the analysis whereas the spallogenic ^{3}He (introduced in these experiments during proton irradiation) is present for analysis. Both Reiners and Farley (1999) and Shuster et al. (2004) agree that the high temperature Arrhenian array (where both ^{3}He and ^{4}He diffusion are the same; Shuster et al. 2004) is the dominant and relevant diffusivity for consideration in helium thermochronology. The data from Cherniak and Watson (2009) agree well with the high temperature arrays from Reiners and Farley (1999) and Shuster et al. (2004).

He in zircon and zircon-structure rare earth element orthophosphates

In the past ten years, there have been several studies of the diffusion of helium in zircon (Table 3 and Fig. 4), mainly from the perspective of interests in thermochronology (Reiners et al. 2002, 2004; Cherniak et al. 2009). There is good agreement amongst these studies, including the observation of marked diffusional anisotropy between *c*-axis parallel and perpendicular measurements. Hourigan et al. (2005) discussed the possible effects of diffusional anisotropy as well as compositional heterogeneity (i.e., distribution of helium-generating parent elements such as U and Th) in the calculation of bulk grain U/Th-He zircon ages and effective closure temperatures. This diffusional anisotropy was confirmed and measured directly by Cherniak et al. (2009).

In addition, Farley (2007) used synthetic rare-earth-element orthophosphates which are isostructural with zircon to evaluate compositional trends of He diffusion in these minerals. Farley (2007) shows that, within these zircon structure orthophosphates, there is a compositional dependence that may be related to ionic porosity (cf. Fortier and Giletti 1989) wherein activation energies

Table 2. Diffusion of helium in titanite.

Species	T (K)	E_a (kJ/mol)	±	D_0 (m^2/s)	log $D_0^\dagger$	±	log D_0/a^2	a (μm)	Notes	References
^{3}He	623-803	183.7	1.4	1.34E-02	–1.87	0.1	5.79	148	a,c	Shuster et al. (2004)
^{4}He	623-803	183.0	1.5	8.46E-03	–2.07	0.1	5.59	148	a	Shuster et al. (2004)
^{3}He	525-873	143	7	8.70E-07	–6.06	na	na	na	b,d,e	Cherniak and Watson (2009)
^{4}He	603-823	186.7	7.1	6.00E-03	–2.22	na	na	na	a	Reiners and Farley (1999)

all diffusivities for vaccuum pressures, except as noted; all uncertainties given at 1σ.

†Many studies give only D_0/a^2; in these cases D_0 is calculated from D_0/a^2 and reported grain size "a" as indicated.

Notes: a - projector lamp step heating and mass spectrometric analysis; b - nuclear reaction analysis depth profiling; c - proton bombardment produced ^{3}He; d - implanted helium; e - 1 atm furnace degassing experiment

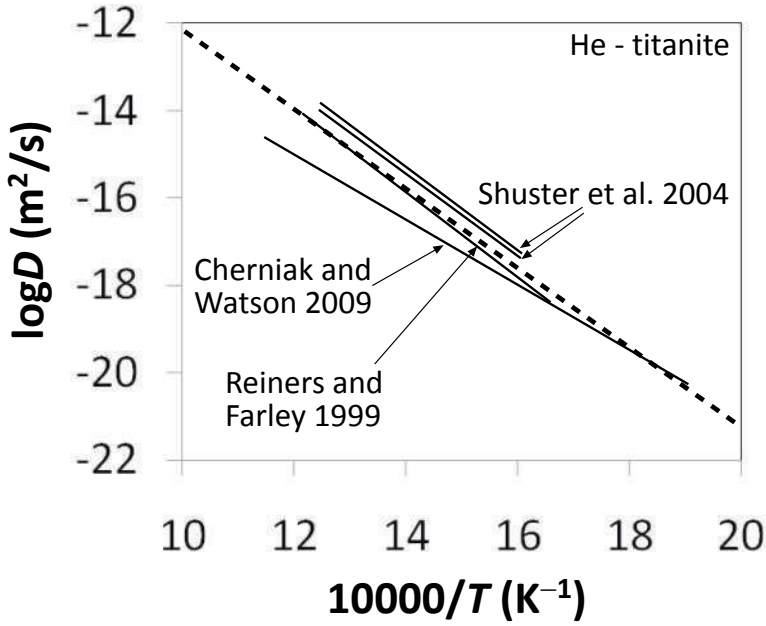

Figure 3. Diffusion data for helium in titanite. Solid lines are data reported from references indicated. Dashed line is the average representative Arrhenius relationship given in Table 9. Shuster et al. (2004) and Reiners and Farley (1999) employ bulk degassing while Cherniak and Watson (2009) employ depth profiling analysis.

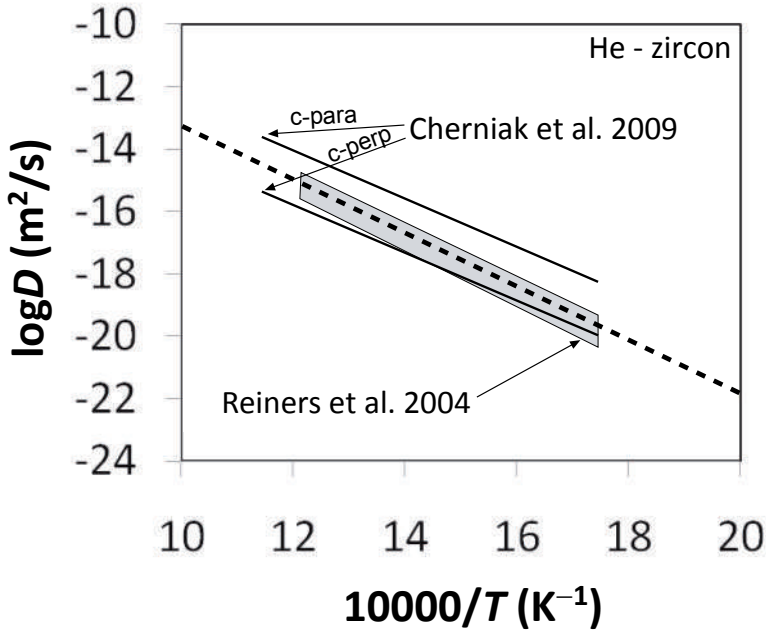

Figure 4. Diffusion data for helium in zircon. Solid lines are from Cherniak et al. (2009) depth profiling analysis. Gray area represents full span of linear Arrhenius relationships from multiple bulk degassing experiments by Reiners et al. (2004). Dashed line is the average representative Arrhenius relationship given in Table 9.

remain constant for all compositions (and ionic porosity) but D_0 varies systematically with ionic porosity. These data thus support the idea of an ionic porosity compositional influence on mineral diffusion, though its significance relative to other compositional or structural effects is not clear. For example, as discussed in Farley (2007) and Cherniak et al. (2009), the absolute magnitude of diffusion in these zircon-structure orthophosphates is markedly higher—by several orders of magnitude—than the actual (silicate) zircon. Reasons for this large difference are unclear, but presumably relate to one or both of the differences between the zircons and orthophosphates studied: 1) coupled substitution of P for Si and REE for Zr in the structure which gives rise to very different crystal-chemical characteristics, or, 2) the fact that the Farley (2007) minerals were synthetic whereas the Cherniak et al. (2009) and Reiners et al. (2002, 2004) minerals were natural. However, this latter possibility (i.e., faster diffusion in synthetic vs. natural materials) is inconsistent with observations of He diffusion in apatite (e.g., Shuster

Table 3. Diffuson of helium in zircon and zircon structure orthophosphates

Mineral	Species	Orientation	T (K)	E_a (kJ/mol)	±	D_0 (m²/s)	log D_0†	±	log D_0/a^2	a (μm)	Notes	Reference
zircon	^{4}He	bulk	553-873	184.6	na	na	na	na	5.64	na	a,f	Reiners et al. (2002)
zircon	^{4}He	bulk	553-873	180.8	na	na	na	na	6.60	na	a,f	Reiners et al. (2002)
zircon	^{4}He	bulk	553-873	153.2	na	na	na	na	2.94	na	a,f	Reiners et al. (2002)
zircon	^{4}He	bulk	553-873	144.8	na	na	na	na	2.89	na	a,f	Reiners et al. (2002)
zircon	^{4}He	bulk	553-873	154.5	na	na	na	na	3.54	na	a,f	Reiners et al. (2002)
zircon (average)	^{4}He	bulk	573-823	169	3.8	4.60E-05	−4.34	0.46	na	na	a,f	Reiners et al. (2004)
zircon	^{4}He	bulk	573-823	173	1.1	8.39E-05	−4.08	0.16	4.71	40	a,f	Reiners et al. (2004)
zircon	^{4}He	bulk	573-823	172	0.3	1.51E-04	−3.82	0.15	4.69	56	a,f	Reiners et al. (2004)
zircon	^{4}He	bulk	573-823	163	0.5	3.08E-05	−4.51	0.30	3.85	66	a,f	Reiners et al. (2004)
zircon	^{4}He	bulk	573-823	170	0.3	5.60E-05	−4.25	0.17	3.75	100	a,f	Reiners et al. (2004)
zircon	^{4}He	bulk	573-823	168	0.3	9.27E-06	−5.03	0.17	3.82	38	a,f	Reiners et al. (2004)
zircon	^{4}He	bulk	573-823	174	0.5	2.70E-05	−4.57	0.27	4.22	40	a,f	Reiners et al. (2004)
zircon	^{3}He	*c*-perp	573-873	146	11	2.27E-07	−6.65	0.80	na	na	b,d,e	Cherniak et al. (2009)
zircon	^{3}He	*c*-para	573-873	148	17	1.67E-05	−4.78	1.32	na	na	b,d,e	Cherniak et al. (2009)
Dy-orthophosphate	^{3}He	*c*-para	408-693	128	4	9.48E+00	0.98	0.26	na	na	a,c	Farley (2007)
Er-orthophosphate	^{3}He	*c*-para	408-693	121	5	3.64E-01	−0.44	0.28	na	na	a,c	Farley (2007)
Ho-orthophosphate	^{3}He	*c*-para	408-693	116	4	2.95E-01	−0.53	0.24	na	na	a,c	Farley (2007)
Lu-orthophosphate	^{3}He	*c*-para	408-693	116	4	3.55E-03	−2.45	0.19	na	na	a,c	Farley (2007)
Tb-orthophosphate	^{3}He	*c*-para	408-693	125	4	4.00E+01	1.60	0.24	na	na	a,c	Farley (2007)
Tm (med)-orthophosphate	^{3}He	*c*-para	408-693	125	4	8.10E-01	−0.09	0.20	na	na	a,c	Farley (2007)
Tm (short)-orthophosphate	^{3}He	*c*-para	408-693	127	4	8.27E-01	−0.08	0.21	na	na	a,c	Farley (2007)
Yb (long)-orthophosphate	^{3}He	*c*-para	408-693	121	3	3.88E-02	−1.41	0.19	na	na	a,c	Farley (2007)
Yb (med)-orthophosphate	^{3}He	*c*-para	408-693	116	3	3.76E-02	−1.42	0.19	na	na	a,c	Farley (2007)
Yb (short)-orthophosphate	^{3}He	*c*-para	408-693	110	3	1.79E-02	−1.75	0.17	na	na	a,c	Farley (2007)
Y-orthophosphate	^{3}He	*c*-para	408-693	123	3	1.36E+00	0.13	0.17	na	na	a,c	Farley (2007)

all diffusivities for vaccuum pressures, except as noted; all uncertainties given at 1σ

†Many studies give only D_0/a^2; in these cases D_0 is calculated from D_0/a^2 and reported grain size "a" as indicated.

Notes: a - projector lamp step heating and mass spectrometric analysis; b - nuclear reaction analysis depth profiling; c - proton bombardment produced helium; d - implanted helium; e - 1 atm furnace degassing experiment; f - post high-T data only

and Farley 2009), where diffusion is slower in synthetic material. In addition, studies of cation diffusion in zircon indicate that diffusion is similar for natural and synthetic materials (Cherniak 2010). A further possibility (pointed out by Cherniak et al. 2009) might be some effects on the synthetic material by the Pb pyrophosphate fluxes (e.g., flux inclusions) used in crystal growth of the REE phosphates. Like the zircon data of Cherniak et al. (2009), these data also reveal strong anisotropy with more rapid *c*-axis parallel channels likely dominating diffusive transport (though Farley (2007) reports only bulk average diffusivities presumably dominated by *c*-axis diffusion).

Lastly, recent molecular dynamics simulations have been developed and directed towards quantifying the diffusion of helium in zircon (e.g., Reich et al. 2007; Saadoune et al. 2009). As discussed in Cherniak et al. (2009) and Cherniak (2010), these efforts have not yet yielded diffusivities which corroborate direct experimental determinations. With further refinements of these molecular dynamic models in the coming years, new insights into helium diffusion in zircon (or within any phase) might be gained.

He in monazite and monazite-structure rare earth element orthophosphates

More recently, several studies explore the potential of He in monazite as a low temperature thermochronometer (e.g., Farley and Stockli 2002; Stockli et al. 2005; Boyce et al. 2005; Farley 2007; Cherniak and Watson 2009). The studies of Boyce et al. (2005) and Cherniak and Watson (2009) show good consistency and thus promise for monazite as a thermochronometer. The Farley (2007) study on synthetic monazite structure rare-earth orthophosphates shows the systematic effect of composition (and ionic porosity) in a similar way to zircon structure minerals (above), only the effect for monazite was seen both in activation energies and pre-exponential factors. Boyce et al. (2009) have pioneered the use of *in situ* laser spot analysis of monazites to conduct U-Th/He thermochronometry even on compositionally zoned (and/or age-zoned) grains. Monazite data are shown in Table 4 and Figure 5.

He diffusion in other minerals

Table 5 shows helium diffusion data for other minerals. Helium diffusion in the context of potential for thermochronology has been explored in magnetite (Blackburn et al. 2007), garnet (Dunai and Roselieb 1996; Aciego et al. 2003 [but also see Blackburn and Stockli 2006 and Aciego et al. 2006]; Roselieb et al. 2006), goethite (Shuster et al. 2005), and hematite (Bahr

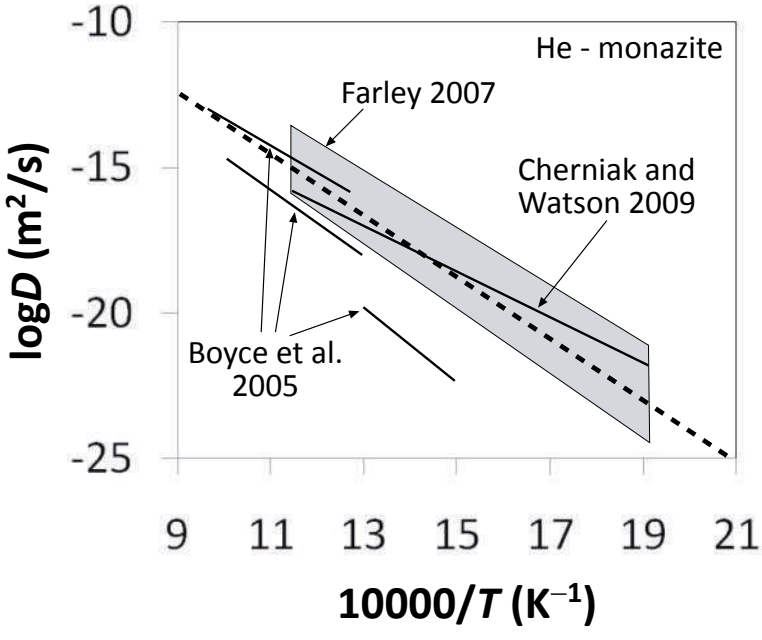

Figure 5. Diffusion data for helium in monazite. Solid lines are for Cherniak and Watson (2009) depth profiling and Boyce et al. (2005) bulk degassing. Gray area represents full span of linear Arrhenius relationships from multiple bulk degassing experiments by Farley (2007). Both Boyce et al. (2005) and Farley (2007) explored a wide range of monazite compositions, which accounts for the spread in the data. The dashed line is the average representative Arrhenius relationship given in Table 9.

Table 4. Diffusion of helium in monazite and monazite structure orthophosphates.

Mineral	Species	Orientation	T (K)	E_a (kJ/mol)	±	D_0 (m²/s)	log D_0†	±	log D_0/a^2	a (μm)	Notes	Reference
monazite	^{3}He	100 norm	525-873	150	11	1.60E-07	–6.80	na	na	na	a,d,f	Cherniak & Watson (2009)
monazite	^{4}He	bulk	670-770	248	11	1.10E-03	–2.96	0.78	11.90	0.037	b	Boyce et al. (2005)
monazite	^{4}He	bulk	788-1037	179.6	1.2	1.20E-04	–3.92	0.07	3.33	238	b	Boyce et al. (2005)
monazite	^{4}He	bulk	771-997	216.5	4.9	4.90E-04	–3.31	0.24	4.92	77	b	Boyce et al. (2005)
Ce-orthophos.	^{3}He	*c*-para	523-873	196	7	2.00E-02	–1.70	0.24	na	na	c,e	Farley (2007)
Gd-orthophos.	^{3}He	*c*-para	523-873	198	7	3.00E-04	–3.52	0.22	na	na	c,e	Farley (2007)
La-orthophos.	^{3}He	c-para	523-873	183	7	1.82E-03	–2.74	0.22	na	na	c,e	Farley (2007)
Nd-orthophos.	^{3}He	c-para	523-873	224	8	8.96E-01	–0.05	0.30	na	na	c,e	Farley (2007)
Pr-orthophos.	^{3}He	c-para	523-873	206	7	7.35E-02	–1.13	0.24	na	na	c,e	Farley (2007)
Sm-orthophos.	^{3}He	c-para	523-873	215	8	1.22E-03	–2.91	0.30	na	na	c,e	Farley (2007)

all diffusivities for vaccuum pressures, except as noted; all uncertainties given at 1σ.

†Many studies give only D_0/a^2; in these cases D_0 is calculated from D_0/a^2 and reported grain size "a" as indicated.

Notes: a - nuclear reaction analysis depth profiling; b - resistance furnace and mass spectrometry; c - projector lamp step heating and mass spectrometry; d - implanted helium; e - proton bombardment produced helium; f - 1 atm furnace degassing

Table 5. Diffusion of helium in other minerals.

Mineral	Species	T (K)	E_a (kJ/mol)	±	D_0 (m²/s)	log D_0†	±	log D_0/a^2	a (μm)	Notes	Reference
augite	^{4}He	453-1123	116	7	4.79E-06	–5.32	0.52	na	na	b	Lippolt and Weigel (1988)
augite	^{4}He	453-1123	124	7	4.47E-06	–5.35	0.49	na	na	b	Lippolt and Weigel (1988)
beryl	^{4}He	923-1823	293	8	na	na	na	na	na	b	Toyota and Ozima (1988)
diamond (carbonado)	^{4}He	623-1873	103.5	4.8	6.31E-18	–17.20	0.2	na	na	b	Zashu and Hiyagon (1995)
diopside	^{4}He	1043-1443	290	40	1.26E-02	–1.90	1.2	na	na	b	Trull and Kurz (1993)
Garnet (py55al40gr4sp1)	^{4}He	1073-1263	660	(+190, -120)	3.98E+11	11.60	(+8, –5.2)	na	na	a	Dunai and Roselieb (1996)
goethite	^{3}He	323-523	162.8	2.4	4.89E-02	–1.31	0.3	11.3	0.50	c,e	Shuster et al. (2005)
goethite	^{4}He	323-523	178.4	2.6	5.00E-01	–0.30	0.3	12.3	0.50	c	Shuster et al. (2005)
hematite (botryoidal)	^{4}He	~423-523	165	17	4.00E-01	–0.40	1.6	7	200	b	Bahr et al. (1994)
hematite (botryoidal)	^{4}He	~423-523	214	9	1.43E+04	4.15	1	13.2	30	b	Bahr et al. (1994)
hematite (botryoidal)	^{4}He	~423-523	180	10	7.91E-02	–1.10	1.5	9.5	5	b	Bahr et al. (1994)
hematite (botryoidal)	^{4}He	~423-523	184	12	6.34E+02	2.80	1.3	10.2	200	b	Bahr et al. (1994)

Table 5 continued on facing page

Mineral	Species	T (K)	E_a (kJ/mol)	±	D_0 (m²/s)	log D_0†	±	log D_0/a^2	a (μm)	Notes	Reference
hematite (botryoidal)	^{4}He	~423-523	173	10	5.68E-01	–0.25	1.1	8.8	30	b	Bahr et al. (1994)
hematite (botryoidal)	^{4}He	~423-523	127	6	9.95E-07	–6.00	2	4.6	5	b	Bahr et al. (1994)
hematite (specular)	^{4}He	~423-1173	127	7	1.00E-09	–9.00	0.4	–1.6	200	b	Bahr et al. (1994)
hematite (specular)	^{4}He	~423-1173	134	12	1.80E-09	–8.74	0.7	–0.3	60	b	Bahr et al. (1994)
hematite (specular)	^{4}He	~423-1173	124	1	1.92E-10	–9.72	0.1	–1.8	110	b	Bahr et al. (1994)
hornblende	^{4}He	453-1123	104	2	9.55E-08	–7.02	0.15	na	na	b	Lippolt and Weigel (1988)
hornblende	^{4}He	453-1123	120	4	1.23E-06	–5.91	0.34	na	na	b	Lippolt and Weigel (1988)
ilmenite	^{4}He	673-1473	46.2	na	4.97E-15	–14.30	na	na	na	b,f	Futagami et al. (1993) (D_0 from Ozima and Podosek 2002)
langbeinite	^{4}He	453-1123	126	5	7.59E-05	–4.12	0.35	na	na	b	Lippolt and Weigel (1988)
magnetite IDPs	^{3}He	1073-1473	80	4	na	na	na	na	na	b	Hiyagon (1994)
magnetite	^{4}He	623-893	220	(+9,-13)	3.94E-01	–0.40	(+.7, –.5)	6.8	250	c	Blackburn et al. (2007)
Muscovite	^{4}He	453-1123	87	10	1.15E-08	–7.94	0.71	na	100-157	b	Lippolt and Weigel (1988)
nepheline	^{4}He	453-1123	88	6	1.15E-08	–7.94	0.46	na	50-100	b	Lippolt and Weigel (1988)
nepheline	^{4}He	453-1123	134	3	2.34E-07	–6.63	0.22	na	50-100	b	Lippolt and Weigel (1988)
nepheline	^{4}He	453-1123	128	5	5.62E-07	–6.25	0.35	na	50-100	b	Lippolt and Weigel (1988)
olivine	^{4}He	673-873	129.8	na	2.00E-08	–7.70	na	na	na	b,f	Futagami et al. (1993) (D_0 est. from data)
olivine	^{4}He	1453-1733	502	(+134, -113)	2.20E+04	4.34	na	na	na	b	Hart (1984)
olivine	^{3}He	553-893	139.6	0.835	5.55E-07	–5.92	0.06	0.40	470[g]	c,e	Shuster et al. (2004)
olivine	^{3}He	423-873	105	17	2.00E-08	–7.70	0.8	na	na	b	Trull et al. (1991)
olivine	^{4}He	1238-1658	420	20	1.26E+01	1.10	0.7	na	na	b	Trull and Kurz (1993)
quartz	^{3}He	423-873	105	4	1.58E-04	–3.80	0.4	na	na	b	Trull et al. (1991)
quartz	^{3}He	343-673	84.5	0.6	1.22E-02	–1.91	0.07	4.82	430	c,e	Shuster and Farley (2005)
quartz	^{4}He	343-673	83.2	0.4	9.06E-03	–2.04	0.07	4.69	430	c,e	Shuster and Farley (2005)
sanidine	^{4}He	453-1123	70	2	6.76E-10	–9.17	0.15	na	50-70	b	Lippolt and Weigel (1988)
sanidine	^{4}He	453-1123	96	4	3.47E-08	–7.46	0.36	na	57-250	b	Lippolt and Weigel (1988)
sanidine	^{4}He	453-1123	92	4	5.89E-08	–7.23	0.39	na	40-50	b	Lippolt and Weigel (1988)

all diffusivities for vaccuum pressures, except as noted; all uncertainties given at 1σ

†Many studies give only D_0/a^2; in these cases D_0 is calculated from D_0/a^2 and reported grain size "a" as indicated.

Notes: a - 25 Mpa pressure internally heated pressure vessel in diffusion experiments; b - resistance furnace step heating and mass spectrometric analysis; c - projector-lamp step heating and mass spectrometric analysis; d - bulk degassing and mass spectrometric analysis; e - proton bombarment produced helium; f - implanted helium; g - correct "a" from Blard et al. (2008)

et al. 1994). The work of Futagami et al. (1993) explored the retentivity of helium (and Ne and Ar) within several phases in lunar soils. He diffusion in andradite garnet and epidote was explored in an abstract by Nicolescu and Reiners (2005). He diffusion in rutile is described in abstracts by Stockli et al. (2005) and Cherniak and Watson (2010). ^{3}He diffusion, including applications to cosmogenic ^{3}He retention and surface exposure age dating, has been explored in quartz (Shuster and Farley 2005; Trull et al. 1991) and olivine (Trull et al. 1991; Shuster et al. 2004). Most other studies of helium diffusion have been conducted within the scientific framework of interpreting mantle evolution and degassing history. These include several studies of He diffusion in diamond (Ozima 1989; Weins et al. 1994; Zashu and Hiyagon 1995 and earlier references therein) olivine (Hart 1984; Trull and Kurz 1993), pyroxene (Lippolt and Weigel 1988; Trull and Kurz 1993), and even subducted interplanetary dust particles (IDPs) with "solar" ^{3}He (Hiyagon 1994). Trull and Kurz (1993) show that ^{3}He diffuses only marginally faster than ^{4}He, and thus that diffusive fractionation of these two isotopes is unlikely in the solid state, though a study by Harrison et al. (2004) may have observed such an effect. A further discussion of helium (and argon) diffusion in mantle minerals is provided in a later section on "suggestions for future study."

Table 6. Diffusion of argon in all minerals. *(continued on facing page)*

Mineral	Species	Orientation	T (K)	P (MPa)	E_a (kJ/mol)	±
Ba silicates	^{39}Ar, ^{37}Ar	bulk	720–1720	vaccuum	~180	na
beryl	Ar	bulk	923–1823	vaccuum	209.3	8.4
beryl	Ar	bulk	923–1823	vaccuum	301.4	25
beryl	Ar	bulk	923–1823	vaccuum	326.5	21
biotite (Ann_{56})	^{40}Ar	bulk	823–1023	100 MPa (2 at 1400 MPa)	197.2	6.3
biotite (Ann_{71})	^{40}Ar	bulk	823–973	100 MPa (2 at 1400 MPa)	211.4	9.2
biotite (phlog)	^{40}Ar	bulk	873–1148	100–200 MPa	242.4	11
corundum	Ar	many	698–1473	0.05–600 MPa	33	3.5
enstatite	Ar	many	698–1473	0.05–600 MPa	32	2.5
hornblende	^{40}Ar	bulk	1023–1173		276.3	16.7
hornblende	^{40}Ar	bulk	1023–1123	100 MPa	251–272	na
ilmenite	Ar	bulk	773–1673	vaccuum	92.4	na
muscovite	^{40}Ar	bulk	873–1003	1000–2000 MPa	263.7	29.3
olivine	^{40}Ar	bulk	673–1673	vaccuum	134	na
olivine (Fo_{100})	Ar	many	698–1473	0.05–600 MPa	42	1
orthoclase	^{40}Ar	bulk	773–1073	200 MPa or vaccuum	183.3	4.2
orthoclase	^{40}Ar	na	793–993	vaccuum	198.2	10.5
orthoclase	^{40}Ar	na	998–1292	vaccuum	268	14.3
orthoclase	^{40}Ar	bulk	na	vaccuum	192.6	25.1
orthoclase	^{40}Ar	na	692–1097	vaccuum	148	na
orthoclase	^{40}Ar	na	762–1097	vaccuum	34.4	na
plagioclase	^{39}Ar, ^{37}Ar	bulk	973–1273	vaccuum	155.3	3.1
plagioclase	^{39}Ar, ^{37}Ar	bulk	973–1273	vaccuum	161.2	2.5
plagioclase	^{39}Ar, ^{37}Ar	bulk	973–1273	vaccuum	178.4	2.1
plagioclase	^{39}Ar, ^{37}Ar	bulk	973–1273	vaccuum	170.8	2.7
plagioclase	^{39}Ar, ^{37}Ar	bulk	973–1273	vaccuum	176.3	6.1
quartz	Ar	many	698–1473	0.05–600 MPa	43	3

all uncertainties given at 1σ.

†Many studies give only D_0/a^2; in these cases D_0 is calculated from D_0/a^2 and reported grain size "a" as indicated.

ARGON

Table 6 lists argon diffusion data in minerals. The study of argon diffusion in minerals consists mostly of investigations related to K/Ar and Ar/Ar thermochronology, and dates back to some of the earliest developmental work in K/Ar geochronology (see McDougall and Harrison 1999 for a review of this early work). Much of the earliest experimental work on argon diffusivity was focused on K-rich minerals including biotite and potassium feldspar. As discussed in McDougall and Harrison (1999) much of the early work suffered from experimental and analytical limitations, including the fact that studies of high temperature argon diffusion in vacuum led to structural breakdown of hydrous phases (e.g., biotite, hornblende). The work of Giletti (1974) first employed a hydrothermal cell to study biotite diffusion. Foland (1974) conducted hydrothermal heating of potassium feldspar. Broadly similar hydrothermal methods have been used in several subsequent studies of diffusion in mica and hornblende (e.g., Harrison 1981, Harrison et al. 1985, Baldwin et al. 1990, Grove and Harrison 1996, Harrison et al. 2009). However, Villa (2010), Villa et al. (1996), and Villa and Puxeddu (1994) have shown that mineral dissolution, including breakdown of mineral impurities, may play a major role in the bulk release of Ar during hydrothermal experiments

D_0 (m^2/s)	$\log D_0$†	±	$\log D_0/a^2$	a (μm)	Notes	Reference
na	na	na	na	na	a,h	Hetherington and Villa (2007)
na	na	na	na	na	a	Toyota and Ozima (1988)
na	na	na	na	na	a	Toyota and Ozima (1988)
na	na	na	na	na	a	Toyota and Ozima (1988)
7.50E–06	–5.12	(+.21, –.14)	na	na	b,c,f,h	McDougall and Harrison (1999)
4.00E–05	–4.40	0.52	na	na	b,c,f,h	Grove and Harrison (1996)
7.50E–05	–4.12	(+.48, –.29)	na	na	c,f	Giletti (1974)
1.20E–20	–19.92	0.15	na	na	d,g	Thomas et al. (2008)
1.30E–20	–19.89	0.15	na	na	d,g	Thomas et al. (2008)
6.00E–06	–5.22	(+.88, –.08)	na	na	c,f	Harrison (1981)
		na	na	na	c,f	Baldwin et al. (1990)
10.00E–15	–14.00	na	na	na	a,i	Futagami et al. (1993) (D_0 from Ozima & Podosek 2002)
2.30E–04	–3.64	(+1.5, –1.4)	na	na	b,c,f,h	Harrison et al. (2009)
5.00E–13	na	na	na	na	a,i	Futagami et al. (1993) (D_0 est. from data)
7.20E–20	–19.14	0.05	na	na	d,g	Thomas et al. (2008)
9.80E–07	–6.01	0.21	na	na	c,f	Foland (1974)
3.74E–06	–5.43	0.6	na	na	e,g	Wartho et al. (1999)
5.50E–03	–2.26	0.7	na	na	e,g	Wartho et al. (1999)
na	na	na	na	na	b	Lovera et al. (1997)
1.70E–09	na	na	na	na	e,g	Kelley et al. (2008); Clay et al. (unpub.)
6.80E–19	–18.17	na	na	na	e,g	Kelley et al. (2008); Clay et al. (unpub.)
1.31E–05	–4.28	0.15	1.72	500	b,h	Cassatta et al. (2009)
2.87E–05	–6.11	0.11	2.06	500	b,h	Cassatta et al. (2009)
6.58E–05	–5.75	0.10	2.42	500	b,h	Cassatta et al. (2009)
1.34E–04	–1.26	0.13	2.73	500	b,h	Cassatta et al. (2009)
9.08E–06	–1.83	0.37	1.56	500	b,h	Cassatta et al. (2009)
3.10E–19	–18.51	0.15	na	na	d,g	Thomas et al. (2008), Watson and Cherniak (2003)

Notes: a – resistance furnace step heating & mass spectrometric analysis; b – laser step heating & mass spectrometric analysis; c – bulk degassing & mass spectrometric analysis; d – Rutherford Backscattering Analysis depth profiling; e – laser depth profiling; f – hydrothermal degassing experiment; g – pressure vessel in–diffusion experiment; h – neutron irradiation produced argon; i – implanted argon

and caution as to their interpretation as pure Fickian diffusion. Grove and Harrison (1996) and Harrison et al. (2009) also report some dissolution-precipitation features in biotites and muscovites (respectively) from their hydrothermal studies, but they estimate that <1% and <5% (respectively) of the total volume of mica is due to new recrystallization. Most diffusion studies of argon involve either bulk loss experiments (such as the hydrothermal experiments above) or step-heating analysis of mineral grains in a resistance furnace or by direct laser heating (e.g., Lovera et al. 1997; Cassata et al. 2009). While several studies have made use of laser ablation noble gas mass spectrometry to explore the distribution of argon within minerals (e.g., Toyota and Ozima 1988; Onstott et al. 1991; Hames and Hodges 1993; Kelley et al. 1994; Reddy et al. 1996, 1999, 2001; Pickles et al. 1997; Kramer et al. 2001; Mulch et al. 2002) it was not until the work of Wartho et al. (1999) that this method was used to extract direct depth profile measurements of Ar diffusion to quantify Arrhenius diffusion parameters, in this case for a gem quality orthoclase. Unfortunately, laser depth profiling has not been successful on micas (in large part because of the sheet structure which does not hold up well to the laser) nor has any laser data for amphiboles been published. Recent work has employed even finer scale laser depth profiling in both quartz and feldspar where the excimer (193-nm) laser permits sub-micrometer depth resolution (Kelley et al. 2008; Clay et al. 2010). Lastly, much recent work has employed Rutherford Backscattering (RBS) analysis to directly measure argon depth profiles at the scale of 10's to 100's of nanometers depth (e.g., Watson and Cherniak 2003; Thomas et al. 2008). The RBS studies have yielded diffusion data that differs from step-heating bulk release data acquired previously for olivine and quartz.

Pressure. In general, the effects of high pressure have rarely been explored for argon diffusion (or for any noble gas). Harrison et al. (1985) conducted two high pressure hydrothermal studies on biotite which produced an estimate for activation volume of 14 cm^3/mol. More recently, Harrison et al. (2009) conducted a high pressure experiment on muscovite and also determined an activation volume of 14 cm^3/mol. For the range of crustal conditions, this activation volume will result in relatively small differences in diffusivity and related diffusive lengthscales and closure temperatures (also see Watson and Baxter 2007). For example, Harrison et al. (2009) calculate differences in muscovite closure temperature of 20 degrees between 500 MPa (405 °C) and 1000 MPa (425 °C). However, for mantle studies of noble gas transport, the effects of pressure should be more important.

Ar in micas

Experimental hydrothermal diffusion studies in micas include the work of Giletti (1974), Harrison et al. (1985), Grove and Harrison (1996), (for biotite) and Harrison et al. 2009 (for muscovite). Earlier studies of diffusion in micas, including some unpublished theses, are reviewed in McDougall and Harrison (1999). Each of these studies employed a bulk step heating analytical method (as opposed to *in situ* depth profiling). Grove and Harrison (1996) explored and discussed several compositional controls on Ar diffusion in biotite, including the diffusivity enhancing effects of Mg/Fe, F^-, and tetrahedrally coordinated aluminum. Dahl (1996a,b) also discusses compositional trends in Ar diffusivity in biotite by way of ionic porosity and interlayer structural partitioning models. Several other workers have employed laser ablation mass spectrometry to directly measure the spatial distribution of Ar within single grains of mica (e.g., Phillips and Onstott 1988; Onstott et al. 1991; Hames and Bowring 1994; Hodges et al. 1994; Hodges and Bowring 1995; Reddy et al. 1996; Kramer et al. 2001; Mulch et al. 2002). While these studies do not yield quantitative diffusion parameters (Hames and Bowring 1994 did calculate an activation energy), they do contribute to the question of the effective diffusive lengthscale. From these studies it seems that micas may often include structurally bound microdomains (e.g., Harrison et al. 1985) or fast paths (e.g., Villa 2010) that effectively decrease the diffusion lengthscale to less than the macroscopic crystal size. This seems especially true for deformed micas where these subdomains are developed and

evident (e.g., Mulch et al. 2002). Harrison et al. (1985) suggest that biotites in general may be characterized by a maximum effective diffusion lengthscale of about 150 μm, though other studies of natural micas suggest much larger diffusion domains (e.g., Hess et al. 1993) up to and including laser studies that support the macroscopic grain size as the diffusive lengthscale (e.g., Onstott et al. 1991; Hames and Bowring 1994; Hodges et al. 1994). Most likely, there is a range of possible diffusion domain sizes within natural micas and the number and fineness of the domains probably scales with the extent to which a mica has been deformed (increasing the number of discrete domains while decreasing the effective domain size; e.g., Kramer et al. 2001 and Mulch et al. 2002). Possible effects of deformation on diffusion are discussed further in a later section. The recent work of Harrison et al. (2009) on muscovite also showed degassing behavior consistent with multiple diffusion domain sizes in their hydrothermally treated bulk samples. In this case, the authors show that the multiple domain sizes result from imperfect grain size sieving during sample preparation as indicated by SEM observations of run materials, and not due to intracrystalline sub-domain populations.

Ar in amphibole

K-bearing amphiboles are often used in Ar/Ar thermochronometry and thus require some knowledge of diffusion kinetics. Besides the work of Harrison (1981) and Baldwin et al. (1990), there exist no hydrothermal experimental diffusion studies of Ar in amphibole from which quantitative constraints on diffusion parameters have been extracted. Villa et al. (1996) performed hydrothermal experiments on hornblende, applying several modes of analysis including step-heating, IR laser spot heating, and UV-laser depth profiling, but find evidence of fast path diffusion along planar defects (documented via TEM observation) that complicate the bulk Ar diffusion behavior and preclude extraction of quantitative diffusion parameters for lattice diffusion. Villa et al. (1996) also caution that mineral breakdown during hydrothermal experiments can lead to misleading overestimates of diffusivity. McDougall and Harrison (1999) review a significant early literature on vacuum heating experiments on amphibole which they argue yield spurious results due to dehydration during the experiment. Another great challenge with amphiboles is the broad compositional diversity that may affect diffusivity from one amphibole to another. This issue has been explored by way of the ionic porosity model (e.g., Fortier and Giletti 1989) which Dahl (1996b) adopted for Ar diffusion in amphibole. Dahl (1996b) model diverse amphibole compositions and show theoretically that diffusivity can vary enough to create differences in Ar closure temperature as great as ~100 °C. Baldwin et al. (1990) reproduce the essential elements of the Harrison (1981) study (including an activation energy of ~250-270 kJ/mol) and produce results on compositionally different amphiboles consistent with the Dahl (1996b) model. Lee (1993) studied the in vaccuo degassing behavior of hornblende and applied a "short circuit" (i.e., fast path) model to explain the complex patterns of release that could not be accounted for by simple volume diffusion alone. From this approach, Lee (1993) extracts "very rough estimates" of short circuit diffusion parameters with activation ~188 kJ/mol, which is significantly lower than the Baldwin et al. (1990) and Harrison (1981) results. Baldwin et al. (1990) also caution as to the presence of micro-mineral inclusions (for example intergrown phyllosilicates) that serve to reduce the effective diffusion lengthscale and alter the bulk diffusive loss characteristics. Overall, amphibole has proven to be a complex and challenging mineral to study in terms of its diffusive characteristics for argon.

Ar in feldspar

The early bulk diffusion study of Foland (1974) on Ar diffusion in potassium feldspar helped pave the way for the use of this mineral as a thermochronometer. The laser depth profiling study of Wartho et al. (1999) produced diffusivities that were close matches to the data from of Foland (1974), providing validation of both methods as well as the bulk diffusive behavior in general. Wartho et al. (1999) argued that there were two separate Arrhenian relationships, one for high temperatures above about 725 °C and another for lower temperatures, perhaps relating

to different domains. However, the laser depth profiling of the gem-quality Madagascar orthoclase showed no evidence of microdomains within the crystal interior, leading Wartho et al. (1999) to conclude that the effective diffusion lengthscale for the Madagascar K-feldspar is the macroscopic crystal size. More recently, work by Clay et al. (2006), Baxter et al. (2006), and Kelley et al. (2008) has employed laser ablation to depth profile Ar uptake in the same Madagascar K-feldspar used by Wartho et al. (1999). Excimer laser depth profiles reported by Kelley et al. (2008) reveal that there is a pronounced kink in the diffusive uptake of Ar in these potassium feldspars within the outer few micrometers (Fig. 6). Indications of a similar kink (manifested by much higher concentrations in the nearest surface region) was also observed by Wartho et al. (1999) but discarded as a surface adsorbtion effect. The kink, now well resolved by the excimer laser study, suggests that there are two diffusive regimes or pathways within the Madagascar K-feldspar. The slower diffusion pathway (manifested by the steep uptake profile within the outer few micrometers of the sample) has an activation energy much lower than either the Wartho et al. (1999) or the Foland (1974) studies (Fig. 7), but quite similar to that found in recent studies of quartz and other minerals using RBS (Watson and Cherniak 2003; Thomas et al. 2008). These themes are explored further below in the section on multi-path diffusion.

Beyond these studies, research in the diffusive loss of Ar from natural potassium feldspars has been marked by the development of the multi-diffusion domain (MDD) model that was created and refined by Lovera et al. (1989, 1997). Whereas other minerals have also been interpreted as consisting of multiple microdomains within each crystal, no mineral has seen the focus (e.g., Lovera et al. 1989, 1997, 2002), success (e.g., Richter et al. 1991; Heizler and Harrison 1998), and attendant controversy (e.g., Villa 1994; Lee 1995; Parsons et al. 1999; Villa et al. 2006; McLaren et al. 2007; Lee 2009; Villa 2010) of the MDD model more than potassium feldspar. The MDD model is described in greater detail in a later section.

There has also been significant interest in plagioclase as a geo/thermochronometer especially given its commonness in many crustal lithologies (see McDougall and Harrison 1999 and Cassata et al. 2009 for review). In basalts and other mafic rocks, plagioclase represents an attractive avenue for geochronology as opposed to dating polymineralic and/or glassy groundmass. Recent work by Cassata et al. (2009) presents Ar diffusion data from plagioclase using a new low-blank laser heating procedure. Their data (from irradiated natural plagioclase) show that there is some range in diffusion parameters among each feldspar crystal, but thermochronologic results are consistent. Cassata et al. (2009) also report behavior consistent with a single grain-scale diffusion domain (rather than a multi-domain model) though single grain Arrhenian relationships appear to have deviations from linearity (not used by the authors in their regressions) that indicate more complex diffusion processes.

Ar diffusion in other minerals

Other minerals studied include beryl (Toyota and Ozima 1988), corundum (Thomas et al. 2008), diamond (Ozima 1989; which may be compromised by graphitization—see Zashu and Hiyagon 1995), pyroxene (Thomas et al. 2008; Cassata and Renne 2010), ilmenite (Futagami et al. 1993), olivine (Futagami et al. 1993; Thomas et al. 2008), quartz (Watson and Cherniak 2003; Thomas et al. 2008; Clay et al. 2010), Ba-silicates (Hetherington and Villa 2007) and the feldspathoids leucite and nepheline (Wartho et al. 2005). Of these, the study of Thomas et al. (2008) is notable for its use of the RBS technique to directly profile Ar uptake into several minerals during high-temperature experiments. Watson and Cherniak (2003) and Clay et al. (2010) also report RBS data. These data have been met with some controversy in the noble gas community in large part due to the high Ar solubilities (and hence mineral/melt partition coefficients) that are resolved by the very short (100's of nanometers) and steep diffusive uptake profiles. In addition to the solubility data (which seems to have received more attention thus far) these data provide quantitative diffusion parameters for these minerals. As with the

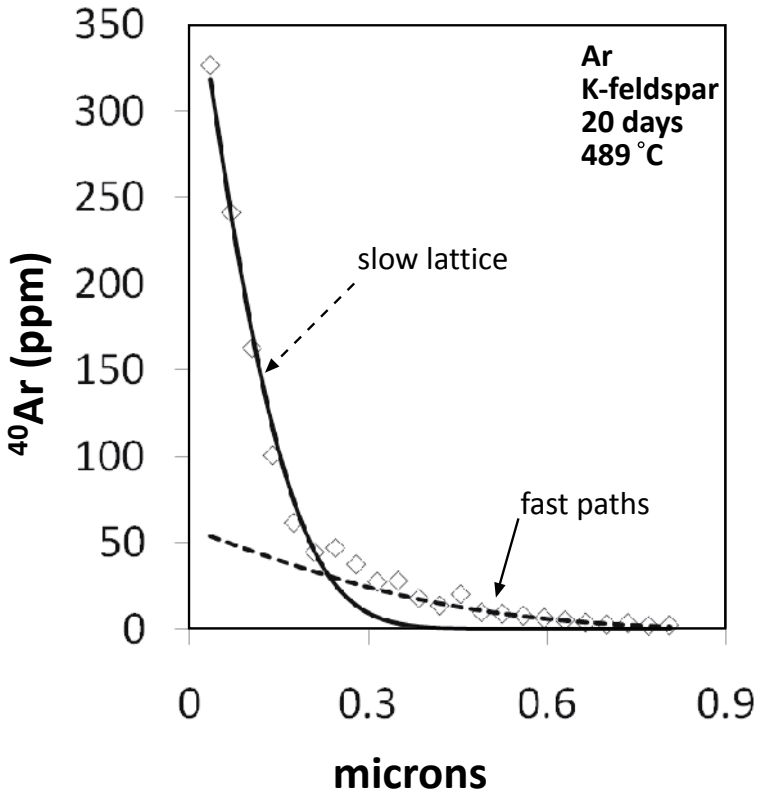

Figure 6. Experimental diffusive uptake profile of argon into potassium feldspar (Madagascar) measured by direct 193-nm (excimer) laser depth profiling (Clay et al. unpub.). These data and other similar profiles formed the basis for the conclusions of Kelley et al. (2008) that two diffusion pathways exist in the Madagascar potassium feldspar. ^{40}Ar concentrations (determined after calibration and measurement of pit depths and volumes) drop steeply in the outer ~200 μm, but the profile kinks and levels off thereafter. The deepest data points (just beyond ~800 μm) still yield significant ^{40}Ar concentrations (>2 ppm) above baseline. Solid line is an error function fit to the first six data only. Dashed line is a fit to the last ten data points only.

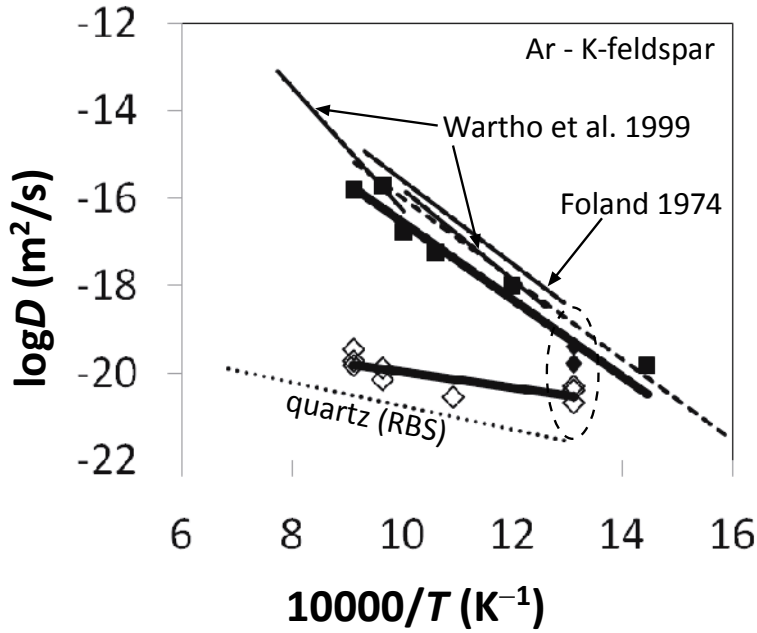

Figure 7. Arrhenius plot of data for argon diffusion in potassium feldspar. Results from bulk step heating of Foland (1974) and the UV-laser depth profiling study of Wartho et al. (1999) are shown as thin solid lines. Thick solid lines are linear fits to the data of Clay et al. (unpub.) analyzed by Kelley et al. (2008) where filled symbols indicate a faster more deeply penetrating diffusion pathway, and open symbols represent a slower more shallowly penetrating pathway. Squares represent data from UV-laser depth profiles and diamonds represent data from 193-nm (excimer) laser depth profiles. Note that in one of these samples (circled: including the profile shown in Fig. 6) both diffusion pathways are captured and resolved in a single excimer laser depth profile. The dashed line is the average representative Arrhenius relationship given in Table 9. Quartz RBS depth profile data of Watson and Cherniak (2003) shown for comparison.

excimer-laser based study of steep diffusive uptake profiles in potassium -feldspar described above (Kelley et al. 2008), each of the minerals studied by Thomas et al. (2008) shows very slow Ar diffusivity with very low activation energies, much lower than any other measurement of Ar diffusion in any mineral by conventional bulk degassing methods (for example, in Fig. 8, compare diffusion of Ar in olivine reported by Futagami et al. (1993) via bulk degassing and Thomas et al. (2008) via RBS depth profiling). One of the many questions left by the recent work of Thomas et al. (2008), Kelley et al. (2008) and Clay et al. (2010) documenting such slow diffusivities with low activation energies, is precisely how these data can be reconciled with the copious thermal bulk degassing data on minerals which give diffusivities with much higher activation energy. This topic is discussed below within the context of multi-path diffusion.

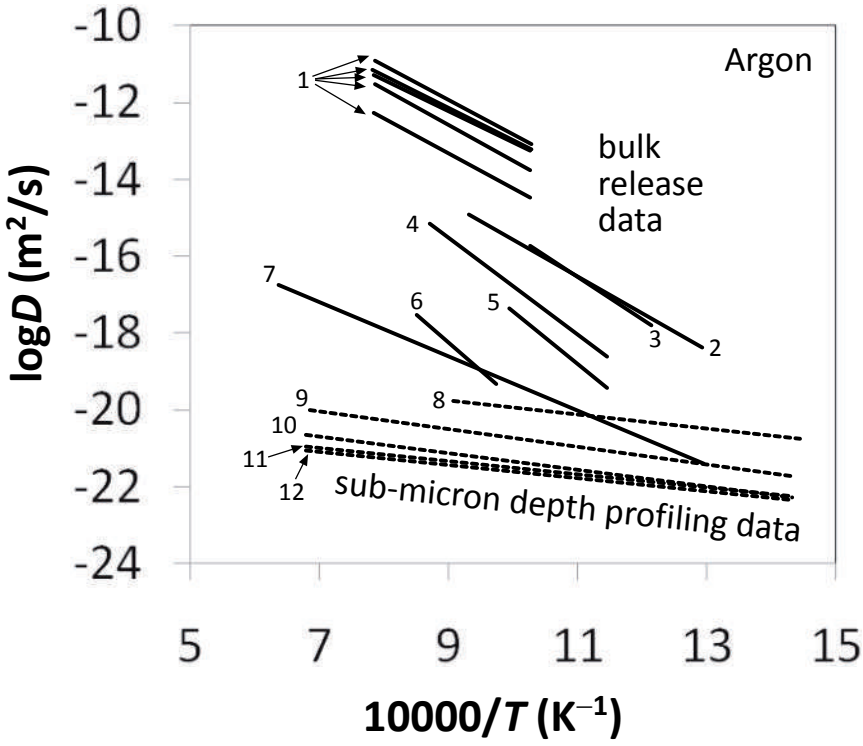

Figure 8. Arrhenius plot of diffusivities measured via direct sub-micrometer resolution RBS or 193-nm (Excimer) laser depth profiling (dashed lines) or via bulk release data (solid lines). Note that all sub-micrometer resolution depth profiling data show markedly lower activation energies as compared to data from bulk release analysis for all silicates. 1) plagioclase (Cassata et al. 2009). 2) orthoclase (Foland 1974), 3) biotite (Grove and Harrison 1996), 4) phlogopite (Giletti 1974). 5) muscovite (Harrison et al. 2009). 6) hornblende (Harrison 1981). 7) olivine (Futagami et al. 1993). 8) orthoclase (193-nm laser; Kelley et al. 2008; Clay et al. unpub.). 9-12) quartz, olivine, enstatite, corundum (RBS; Thomas et al. 2008).

THE OTHER NOBLE GASES: NEON, KRYPTON, XENON, RADON

There are scant data available in the published literature providing quantitative constraints on the diffusivity of the remaining four noble gases in naturally occurring minerals (Table 7). Of the four, neon diffusion has been studied the most. Futagami et al. (1993) report Ne diffusion parameters for lunar soil grains of ilmenite and olivine. Hiyagon (1994) measured the bulk release characteristics of solar neon from IDPs. Shuster and Farley (2005) measured the diffusive kinetics of irradiation induced ^{21}Ne in quartz. While no thermochronologic use of Ne has yet been developed, recent work by Gautheron et al. (2006) shows the potential for U-Th/Ne chronometry in U-Th rich minerals (where Ne isotopes are produced by alpha reactions). No

Table 7. Diffusion of neon and xenon in minerals.

Mineral	Species	T (K)	E_a (kJ/mol)	±	D_0 (m²/s)	log D_0†	±	log D_0/a^2	a (μm)	Notes	Reference
ilmenite	^{20}Ne	673-1473	62.8	na	1.95E-15	na	na	na	na	a,c	Futagami et al. (1993) (D_0 from Ozima and Podosek 2002)
magnetite IDPs	^{20}Ne	1073-1473	106	4	na	na	na	na	na	a	Hiyagon (1994)
olivine	^{20}Ne	673-1673	87.9	na	3.00E-14	na	na	na	na	a,c	Futagami et al. (1993) (D_0 est. from data)
quartz	^{21}Ne	343-673	153.7	0.8	1.49E+00	0.17	0.07	6.90	430	b,d	Shuster and Farley (2005)
Ba silicates	^{131}Xe	720-1720	~300	na	na	na	na	na	na	a,e	Hetherington and Villa (2007)

all data are for bulk diffusion acquired via step heating experiments *in vacuo* and mass spectrometry analysis; all uncertainties given at 1σ.

†Many studies give only D_0/a^2; in these cases D_0 is calculated from D_0/a^2 and reported grain size "a" as indicated.

Notes: a - resistance furnace & mass spectrometric analysis; b - projector-lamp & mass spectrometric analysis; c - implanted noble gas; d - proton bombardment produced ^{21}Ne; e - neutron irradiation produced Ar and Xe

data are found in the literature for krypton, perhaps a testament to the dearth of applications of krypton isotopes in solid earth systems given its six stable and non-radiogenic isotopes. Interest in xenon diffusion exists in the context of the short-lived Pu-Xe and I-Xe chronometers used in studying early solar system processes (e.g., Shukolyukov and Begemen 1996; Swindle 1998; Hohenberg et al. 2004). Such work often focuses on meteorite fragments including altered fine grained polymineralic inclusions (e.g., CAIs) which retain unique Xe-isotopic signatures. Recent work has even shown Xe-isotopic evidence for live ^{244}Pu in the Hadean age Jack Hills zircons (Turner et al. 2007). However, despite this use of Xe isotopes in geochronology, there are little data on Xe diffusion from these materials from which to extract accurate E_a and D_0 (see Swindle 1998), and none on individual mineral phases (as opposed to meteorite fragments consisting of many minerals; e.g., Burkland et al. 1995). The studies by Melcher et al. (1981, 1983) of the retention of ion-implanted Xe in olivine and feldspar report some limits on Xe activation energy. Turner et al. (2007) report that Xe-retention ages are systematically younger than Pb-Pb ages in the Jack Hills zircons, which they suggest is due to loss of Xe, perhaps due to metamictization. The only published study of Xe "diffusion" in minerals is the work of Hetherington and Villa (2007) who irradiated several Ba-rich silicates to study the release characteristics of both Ar and Xe. They report only estimated activation energies for Xe in these minerals, all similar to each other at ~300 kJ/mol despite a wide range of silicate structures, and ascribe the similar behavior to the high temperature structural re-organization (rotation) of silicon tetrahedra as the common mechanism controlling loss of Xe (and Ar) from the diverse silicate structures. As Hetherington and Villa (2007) discuss, the in vacuo degassing behavior of Ar and Xe cannot be the result of simple Fickian diffusion given this structural transformation. Radon, part of the U-series decay chain, is radioactive and short lived (its longest lived isotope is ^{222}Rn with a 3.8 day half-life) so its applications in geosciences do not include chronology and thus generally do not require quantification of the diffusional loss of Rn from minerals. However, there is a vast literature involving consideration of the bulk diffusive transport of radon through soils, faults, and porous media which are important for assessing human health hazards, hydrological flow patterns, and even earthquake prediction (e.g., Trique et al. 1999).

THEMES IN NOBLE GAS DIFFUSION IN MINERALS

The remaining sections of this chapter cover several common themes that have broad relevance for all noble gases, and for many minerals. Many of these concepts have been mentioned in the preceding sections, but here these themes are brought together and discussed further. These themes represent areas, some of which are controversial, ripe for further research in noble gas diffusion in minerals.

Effect of radiation damage

Since most geochronologic applications of noble gas geochemistry involve minerals with high concentrations of radioactive elements, the effect of the lattice damage caused by the kinetic energy of daughter products on noble gas retentivity is an issue which has attracted considerable attention. Concerns over metamictization of (especially) zircons affecting the retentivity of Pb go back to the early days of U-Pb zircon geochronology. With more recent applications of U-Th/He thermochronology, these concerns have been raised anew with regard to the effect of radiation damage on He retentivity in commonly dated minerals including zircon, apatite, and other accessory phases. Based largely upon observations of the effect of metamictization of zircon on Pb retentivity, conventional wisdom would have that He retentivity would decrease as radiation damage accumulates in the crystal lattice, creating more and more extended defects and even amorphization of the material. However, a series of recent observations both in the lab and in nature (e.g., Shuster et al. 2006; Flowers 2009; Flowers et al. 2007, 2009; Gautheron et al. 2009; Shuster and Farley 2009) have shown that in the case of the low temperature diffusivity of helium in apatite (crucial for low-T thermochronology) the opposite seems to be occurring. These studies have shown that the effective bulk diffusivity of helium in apatite decreases as radiation damage accumulates in the mineral, either due to prolonged natural decay of uranium or thorium, or due to artificial neutron irradiation induced radiation damage in some experiments. These authors show that helium retentivity (using measured U/Th-He ages or laboratory diffusion experiments) varies with the age, the thermal history (including specifically the time over which the mineral experienced high enough temperatures to anneal out some or all of the radiation damage; e.g., Shuster and Farley 2009, Gautheron et al. 2009) and the U and Th concentration in the mineral. To account for this phenomenon, Shuster et al. (2006) and Shuster and Farley (2009) suggest that a finite amount of radiation induced damage to the crystal lattice (most likely related to alpha recoil), rather than leading directly to amorphization and fast interconnected pathways, leave "energy wells"—*isolated* defects—into which diffusing helium atoms fall and effectively get held up as they move through the lattice. Presumably, once a certain concentration of radiation damage induced defects has accumulated, amorphization will occur as defects become interconnected and at this point, diffusivities will rapidly increase. The radiation damage and accumulation model (RDAAM) of Flowers et al. (2009) uses the effective fission track density as a proxy for bulk radiation damage to predict the net effect on helium diffusivity and consequently, He-age, as the fission tracks themselves respond to and record the effects of both radiation damage and annealing. It should be noted that there is scatter in the existing experimental data upon which the RDAAM model has been parameterized, indicating second order uncertainties in the underlying physical model that still need to be resolved. In particular, it is unclear whether the averaging together of all radiation damage phenomena contributing to these energy wells is sufficient to capture the net effect on diffusion, especially when applying intense neutron irradiation experiments as an analogy to radiation damage effects under conditions and timescales of relevance in nature. There is also evidence that similar processes may be affecting the diffusivity of other non-noble gas elements (e.g., Pb, Sr) in apatite, zircon, titanite and other minerals with high concentrations of alpha-emitters (e.g., U, Th, Sm), though these relative effects may differ significantly between minerals as damage accumulation, retention, and recovery mechanisms vary (e.g., Cherniak et

al. 1991; Cherniak 1993; Cherniak and Ryerson 1993; Cherniak and Watson 2001; Weber and Ewing 2002). Recent measurement of helium diffusion in apatite via helium implantation and NRA analysis (Cherniak et al. 2009) does not seem to show a significant effect from radiation damage, though these authors point out that one must consider the different varieties of radiation damage that may occur, some of which perhaps may not affect diffusivity at all. For example, the proton-bombardment experiments of Shuster et al. (2004) show no radiation damage effect on helium diffusivities, whereas neutron irradiation leads to significant damage effects (e.g., Shuster and Farley 2009). Furthermore, Cherniak et al. (2009) point out that a synthetic (and therefore presumably radiation damage free) apatite also studied by Shuster and Farley (2009) actually yielded the slowest diffusivities, which would seem to contradict the simple radiation damage and accumulation model of Shuster et al. (2006) which was based largely upon natural Durango apatite. Still, when this synthetic apatite was exposed to radiation damage it too became *more* retentive of helium (Shuster and Farley 2009). Even as absolute diffusivities for different materials vary in ways that may not be fully understood, the *relative* effect of the addition of finite amounts of radiation damage (natural or artificial) seems consistently to be a decrease in diffusivity (i.e., an increase in retentivity). Reasons for the difference in absolute diffusivity between natural and synthetic materials remain generally unclear.

Effect of deformation

In a manner broadly analogous to radiation damage, structural deformation of a mineral due to tectonic or other stresses might also be expected to alter the diffusive retentivity of an element. This seems especially relevant to thermochronology in metamorphic rocks such as schists or mylonites where the dateable minerals (such as micas) experience significant deformation during exhumation (e.g., West and Lux 1993). This topic has been explored experimentally by Dunlap and Kronenberg (2001) and studied in natural samples by Reddy et al. (1996), Heizler et al. (1997), Reddy et al. (1999, 2001), Kramer et al. (2001), Mulch et al. (2002). Dunlap and Kronenberg (2001) experimentally deformed micas and measured their $^{39}Ar/^{40}Ar$ composition before and after the attending deformation. They concluded that plastically deformed (sheared) micas exhibited enhanced bulk diffusive loss as a consequence of reduction of grain size and the effective diffusion lengthscale. They suggest that the effect of deformation on the diffusivity of Ar in mica was negligible (< ~1 %) and thus that the effect of deformation on Ar retentivity was solely a mechanical one. The study of naturally deformed muscovites by Mulch et al. (2002) supports the conclusions of Dunlap and Kronenberg (2001). Mulch et al. (2002) found that the most deformed micas gave the youngest ages due to the development of "*microstructurally controlled segments [that] are bound by either first-order lattice discontinuities, sub-microscopic structural defects and/or zones of high defect density*." The studies by Heizler et al. (1997) and Kramer et al. (2001) also showed that deformed micas exhibited a reduced Ar retentivity and, younger ages, likely due to a mechanical decrease in the effective diffusion lengthscale. Reddy et al. (1996) showed that deformation of biotite also enhanced the diffusivity of argon within those deformed portions of the mineral, only in this case promoting the uptake of excess ^{40}Ar and consequently older ages. Reddy et al. (1999, 2001) documented enhanced argon diffusivity in deformed potassium feldspars, suggesting that deformation could have led to the development of small diffusion domains and a denser network of "short circuit" pathways. Interestingly, radiation damage accumulation (described in the previous section) appears to result in the opposite effect as compared to the addition of mechanical damage related to deformation processes, suggesting that the structural defects produced by radiation damage are different from any defects related to mechanical deformation—perhaps only in their isolated versus interconnected nature, or in their abundance. Lastly, Thomas et al. (2008) in their RBS depth profiling study of argon diffusion in several minerals measure diffusivities with very low activation energies, much lower than any bulk measurements. While they argue that their data indeed represent lattice diffusion, they speculate that the presence of isolated point defects within the lattice (the abundance and distribution of which may have something to do with the strain

history of the mineral grain, as well as an intrinsic defect population related to crystal chemistry and Fe oxidation states) serve to slow the lattice diffusivity as these defects slowly "fill up" as argon penetrates the mineral. While not a perfect analogy, these hypothesized isolated defects and their retarding effect on lattice diffusion are conceptually similar to the radiation damage effects described in other studies for helium.

Multi-domain diffusion

Introducing one of the more controversial topics within thermochronology, Lovera et al. (1989) first formalized the "multi-domain diffusion" or MDD model to describe the behavior of Ar released from potassium feldspar during *in vacuo* heating experiments. The reader is directed to that and subsequent studies for a detailed treatment of the MDD model (e.g., Lovera et al. 1997, 2002). Since then, several other minerals have also displayed characteristics that have been interpreted and/or modeled (at least by some) as multi-domain diffusion (e.g., Ar in multi-grain sized bulk muscovite - Harrison et al. 2009; Ar in amphibole - Baldwin et al. 1990; He in goethite - Shuster et al. 2005; He in calcite - Copeland et al. 2007). Purely from the perspective of diffusion during step-heating analysis, the patterns of bulk release from potassium feldspar and other minerals with purported MDD behavior are, in a word, non-Arrhenian. Several deviations from linearity in the Arrhenius diagram can appear (e.g., Fig. 1). The mathematical and physical interpretation put forth by Lovera et al. (1989) is that these patterns reflect loss of Ar from several discrete populations of intracrystaline domains of different effective diffusional lengthscales. In this model scenario, the only difference between the domains is their diffusional lengthscale, generally described by their effective radius. The diffusivity of Ar within each domain is the same (same activation energy), presumably relating to the lattice diffusivity of potassium feldspar. But while the MDD model has provided a mathematical framework capable of quantifying the diffusive behavior in potassium feldspar (and to exploit it to extract detailed thermal histories from natural samples), questions—and some controversy (e.g., Villa 1994, 2006, 2010; Parsons et al. 1999; McLaren et al. 2007; Lee 2009)—have persisted as to the actual physical nature of these domains which generally have not been corroborated by mineralogists. Indeed, feldspar microtextures can be very complex and can evolve during cooling, alteration, deformation, or laboratory step heating (e.g., Parsons et al. 1999). The question is whether the complexities of natural potassium feldspars can be *adequately* represented by the MDD model. Recent and ongoing collaborative work by Matthew Heizler (an Ar/Ar thermochronologist and MDD modeler; e.g., Heizler and Harrison 1998) and Ian Parsons (a feldspar mineralogist and MDD skeptic; e.g., Parsons et al. 1999) is bringing new insights and reconciliation to the MDD model and its physical and mineralogical bases, as well as its limitations (e.g., Heizler et al. 2008). Part of the persistent skepticism revolves around the fact that the remarkably detailed thermal histories derived from MDD modeling of natural potassium feldspars cannot be directly tested by independent chronometers. Even as higher temperature (e.g., Ar-in-mica) or lower temperature (e.g., He-in-zircon) thermochronometers can be employed to test/corroborate the upper or lower bounds of an MDD model temperature-time path, the second order features of the MDD interpretation are unique and untestable except by corroboration by repeat potassium feldspar analysis. Indeed, this is the power of the MDD potassium feldspar method—that it can provide continuous temperature-time information unavailable by any other means—and hence the primary reason that geoscientists continue to evaluate and question the method at this level of specificity. It has also been shown (e.g., Lee 2009; Shuster et al. 2010) that the MDD model introduces additional physically unknown free parameters (e.g., number of domains, domain sizes, proportion of Ar in each domain) that may expectedly produce a better fit to the bulk release data than a simple single-domain model, but may not necessarily produce a more *accurate* characterization. Lastly, there are several assumptions that would need to be met for the MDD model to hold for application to natural samples. These assumptions (reviewed by Parsons et al. 1999; Lee 2009) include stability of the domains both in nature and experiment, non-interaction of the domains, simple diffusion geometry for each domain, infinite diffusivity

in the inter-domain "fast paths" (i.e., zero concentration boundary condition surrounding each domain), and the crucial assumption that diffusion behavior in the lab mimics the diffusion behavior that occurred in nature. Villa (1994, 2006), Parsons et al. (1999), McLaren et al. (2007) and others have shown that at least some of these assumptions do not always hold (including issues related to complex and/or evolving microtextures that can differ between lab and nature), though this has been a point of contention (e.g., Copeland et al. 1996; Lovera et al. 1996; Villa 1996a,b). Lovera et al. (1997) show MDD modeling interpretations for over 100 feldspars which help document the sensitivity of MDD modeling to any of these potential compromising factors that may exist in a given sample. They argue that most samples exhibit behavior overall consistent with the MDD model, though there exists second order deviations that still require additional explanation.

One thing is certain: potassium feldspar noble gas release patterns (and other minerals exhibiting broadly similar behavior) cannot be explained and understood by simple homogeneous, single-domain, Fickian diffusion models alone. One of the limitations is the reliance on bulk release data (with its inherent uncertainties as described above) and the absence of sub-micrometer scale observations of Ar distribution within purported MDD minerals that would serve to corroborate and elucidate the underlying physics. In the following section, new direct depth profiling of potassium feldspar will be discussed which shows evidence of sub-micrometer scale apparent diffusive heterogeneity that may be related to the MDD behavior. Especially as "MDD-like" effects continue to be observed in feldspar and other minerals, the physical governing basis behind this theoretical model (the "cipher" for the as yet unknown domain structure within these feldspars; cf. McLaren et al. 2007) merits further study.

Multi-path diffusion

Lee (1995) described a theory behind multi-path or fast path diffusion in minerals, again with specific focus on the behavior of Ar noted in thermochronological studies. Additional discussion may be found in Watson and Baxter (2007). The conceptual model is that noble gases can effectively "short circuit" the long trip from a crystal interior through the mineral lattice by exploiting a fast path which provides a quicker way out of the mineral. A noble gas atom, once inside the fast path, would then be able to diffuse along it more rapidly than within the bulk crystal lattice. In one end-member conceptualization, the fast path diffusivity may be effectively infinite, such that once the noble gas gets to the fast path (by diffusing some distance through the mineral lattice to get there) it is lost from the crystal. This is essentially how the MDD model of Lovera et al. (1989) is set up; the MDD model may be thought of an end-member case of multi-path diffusion where the network of pathways separating the domains have infinite diffusivity. However, when the fast path diffusivity is neither infinitely fast nor infinitely capacitive for noble gases, the situation changes somewhat. In such a case, both the fast path and the (relatively slower) lattice diffusion are relevant to describe the overall diffusive behavior. In addition, Lee (1995) uses a set of "exchange coefficients" to describe the movement of argon between fast paths and the lattice. It would seem that this exchange could be described by diffusive exchange governed by chemical potential gradients (i.e., with consideration of the equilibrium partitioning of argon between lattice and fast path) of argon between the lattice and fast path (e.g., Watson and Baxter 2007). Villa (1994) also calls upon a fast-path model to account for Ar diffusion behavior in potassium feldspar. Several studies of amphibole diffusion have also been interpreted as fast path diffusion (Baldwin et al. 1990; Lee 1993; Villa et al. 1996).

Recent experimental data has shown that such multiple pathways (for Ar) can be resolved in quartz and feldspar (Clay et al. 2006; Baxter et al. 2006; Kelley et al. 2008; Clay et al. 2010). Depth profiles of Ar uptake (during high temperature experiments in a pressurized argon vessel) in both quartz and potassium feldspar show two distinct diffusion pathways, evidenced by a pronounced kink in the diffusive uptake profiles (Fig. 6). In quartz (Clay et al. 2010), the two pathways are revealed by comparing RBS depth profiling of the outermost ~200 nanometers

(which shows a very steep and slow diffusive uptake and very high Ar concentrations; Watson and Cherniak 2003 report similar observations) with UV-laser depth profiling of the same samples penetrating tens of micrometers (which show a much more deeply penetrating uptake profile with lower concentrations). In potassium feldspar, the use of a 193-nm (excimer) laser permits sub-micrometer resolution of both pathways using a single analytical approach, obtaining a single profile (Fig. 6) showing both contributions. The marked kink in the profile cannot be modeled with a single pathway (and a single diffusivity). Rather, Kelley et al. (2008) suggest the effects of two distinct diffusion pathways. The nearer-surface region (up to ~0.5 μm depth in these experiments) most likely represents the lattice diffusion of Ar in potassium feldspar, whereas the more deeply penetrating profile likely includes the contributions of some sort of "fast paths" in the feldspar. The lower concentrations of the deeper penetrating profile represent the average of "normal" feldspar lattice with near zero concentration and fast-paths with higher concentrations. Thus, the density, orientation, and distribution of fast paths in a given mineral can lead to variations in the uptake profile. Notably, as shown in Figure 7, the "fast path" diffusivities determined from these data agree well with previous deep depth profiling and bulk degassing experiments on potassium feldspar, whereas the steep and slow lattice diffusivity is similar to that observed for Ar in quartz (measured with RBS, e.g., Watson and Cherniak 2003; Thomas et al. 2008). The effect of isolated point-defects on lattice diffusivity suggested by Thomas et al. (2008) could also be operating in the potassium feldspar.

While quartz and potassium feldspar are the only minerals for which these two diffusion pathways for noble gases have been directly observed via depth profiling, examination of Ar diffusivity data, including RBS analysis (with ~10 nanometer scale resolution), UV-laser depth profiling (with micrometer scale resolution), and bulk release analysis suggest that many minerals may have two (at least) diffusive pathways (Fig. 8). For example, olivine, which has been analyzed via RBS depth profiling (Thomas et al. 2008) and via bulk release (Futagami et al. 1993) shows two quite different results. In general, the RBS studies (and the recent 193-nm excimer laser depth profiling of Kelley et al. (2008) and Clay et al. (unpub.) in potassium feldspar) illuminate a slower pathway with very low activation energies (dashed lines in Fig. 8). The fact that the low activation-energy pathways are now observed in both RBS and sub-micrometer scale 193-nm laser depth profiles indicates that the result is not limited to (or somehow related to) any one particular analytical method. Thomas et al. (2008) present extensive arguments that these diffusive uptake profiles measured in the outermost few hundred nanometers of the crystal indeed represent the slow lattice diffusivity of the mineral, rather than a spurious surface effect related to an anomalous or damaged surface layer. The findings of Watson and Cherniak (2003) in which diffusivities of Ar in quartz were similar despite differences in surface preparation, also support this conclusion. Similar kinks in diffusive uptake profiles have been reported for other elements (e.g., oxygen in titanite; Zhang et al. 2006). All other coarser scale or bulk analyses show faster diffusion with much higher activation energy (solid lines in Fig. 8). It may be that the slower pathway exists in many more minerals but it has not been noticed before because the analytical methods used could not resolve this finer scale feature (or at least in experimental studies on laboratory timescales). The fact that bulk thermal release seems to respond to higher activation energy pathways points to the dominant role of fast paths (the exact physical identity of which are yet to be pinned down) in at least these lab-based experimental degassing studies.

If we accept the existence of these two pathways in at least a few minerals (quartz, olivine, potassium feldspar), the question then becomes which pathway and diffusivity is appropriate for use in the interpretation and modeling of natural minerals and systems. The answer is not clear at present (in large part because the exact identity and underlying physical mechanism for the two pathways remains uncertain), and it may well be that both are relevant simply depending on the timescales, lengthscales, and temperatures of interest. For the specific case of the Madagascar potassium feldspar studied by Wartho et al. (1999) and Kelley et al. (2008), it is difficult to reconcile how these depth profile observations of multi-path diffusion could mesh

with the MDD model of potassium feldspar, especially since the activation energies associated with most MDD feldspars are high (e.g., ~193 kJ/mol of Lovera et al. 1997), consistent with the activation energy for the *faster* pathways of Wartho et al. 1999 (198 kJ/mol) and Kelley et al. 2008 (148 kJ/mol; see Fig. 7), leaving one to wonder about the significance of the low activation energy measured for lattice diffusion—which must describe in some way the lattice characteristics. In the simplest interpretation, this value describes simple unmodified lattice diffusion, or alternatively, it is an effective activation energy that incorporates lattice diffusion coupled with some other physical effect(s) (such as trapping of Ar in point defects in the lattice, as proposed by Thomas et al. 2008). Viewed another way, the observation of two diffusion pathways (neither of which show infinite diffusivity such as the MDD model interdomain network requires) characterized by two different activation energies is contradictory to one of the main assumptions of the MDD model: that each domain has the same activation energy. Another interesting note is that the low-activation energy pathway leads to minerals which will have very broad thermal "closure" intervals because diffusivity doesn't drop rapidly with cooling temperatures. If the low-activation energy pathways are relevant in natural systems (it is difficult to envision how they would not be if they represent the most fundamental mineral lattice transport properties) these minerals would display a very broad "partial retention zone" extending to quite low temperatures. For example, Baxter (2003a) discusses the implications of this slow leaking (or slow uptake) behavior for the case of quartz as a possible crustal storehouse for excess Ar.

Synthesis: relative diffusivities of the noble gases in minerals

Compilation of published data on noble gas diffusion in minerals provides an opportunity to look for broad systematic trends. One such trend is the commonly held notion that the diffusivities of the noble gases scale inversely with their radii; that is, that the heavier gases (with larger radii) diffuse more slowly. And while it is generally true that helium diffuses faster than argon at low temperatures, there is surprisingly little data on all the other noble gases in the same minerals. Table 8 lists all minerals for which there is experimental diffusion data for at least two of the noble gases. Only nine minerals currently have published diffusion data on more than one noble gas, and only three of those minerals (ilmenite, olivine, and quartz) have diffusion data published on three. Of these, only the study by Futagami et al. (1993) (ilmenite and olivine) presents diffusion data for three noble gases (He, Ne, Ar) all determined in the same experiments and with the same analytical methods, though these authors suggest a major role of bubbles in controlling aspects of noble gas release. Only Shuster and Farley (2005) (quartz), Hetherington and Villa (2007) (barium silicates) and Toyota and Ozima (1988) (beryl) report diffusion data for two noble gases from the same study. Even though Hetherington and Villa (2007) caution against the interpretation of their complex release patterns as Fickian diffusion (there is strong evidence for a structural re-organization during degassing), there is value in exploring the *relative* "release" rates of Xe and Ar from their samples. Figure 9 shows the expected systematic relationship between the diffusivity of different noble gases in ilmenite, quartz, and Ba-silicates (at least at low temperatures). Toyota and Ozima (1988) and Futagami et al. (1993) also find the expected relationship for beryl and olivine, respectively. An important observation from three of these studies (excepting the case of beryl and olivine, see below) is that the activation energies also vary systematically for the noble gases, with the heavier noble gas having the highest activation energies. This is the expectation justified on a crystal chemical basis; that activation energy for a diffusive jump from one site or vacancy to the next will scale with atomic radius of the diffusant (e.g., Shuster and Farley 2005). In contrast, the data of Futagami et al. (1993) for olivine appear to show almost identical activation energy for He, Ne, Ar all of which are quite low (~134 kJ/mol, if one spurious datum for Ne is rejected), but the Arrhenius relationship for He is based on just three points. The most recent study of Shuster et al. (2004) as well as Trull et al. (1991) corroborate this low activation energy for helium in olivine (139.6 and 105 kJ/mol, respectively) but two other earlier studies of He diffusion in

Table 8. Number of modern diffusion studies for each mineral and noble gas included in this Chapter's tables.

Mineral	He	Ne	Ar	Kr	Xe
apatite	9	none	none	none	none
augite	1	none	none	none	none
Ba-silicates	none	none	1	none	1
beryl	1	none	1	none	none
biotite	none	none	3	none	none
corundum	none	none	1	none	none
diamond	1	none	none	none	none
diospide	1	none	none	none	none
enstatite	none	none	1	none	none
garnet	1	none	none	none	none
geothite	1	none	none	none	none
hematite	1	none	none	none	none
hornblende	1	none	2	none	none
ilmenite	1	1	1	none	none
langbeinite	1	none	none	none	none
magnetite IDP particles	1	1	none	none	none
monazite	3	none	none	none	none
Muscovite	1	none	1	none	none
nepheline	1	none	none	none	none
olivine	5	1	2	none	none
orthoclase	none	none	4	none	none
plagioclase	none	none	1	none	none
REE orthophosphates	1	none	none	none	none
Quartz	2	1	1	none	none
sanidine	1	none	none	none	none
titanite	3	none	none	none	none
zircon	3	none	none	none	none

Note: other studies exist but either do not provide quantitative constraints on E_a and D_0, or they have been superceded by other work.

olivine give much higher activation energies (420-502 kJ/mol; Trull and Kurz 1993 and Hart 1984) which may be attributed to the higher temperatures (965-1385 °C and 1180-1460 °C, respectively) over which their experiments were conducted or other complicating effects (see discussion in later section). Furthermore, the recent study of Ar in olivine by Thomas et al. (2008) employing RBS analysis yields a much lower activation energy (42 kJ/mol) than for any of these other studies. As discussed above, this is likely because the sub-micrometer scale resolution of the RBS analysis provides a window into a diffusive pathway that is not the same as the pathway(s) represented by these other studies in which bulk release, rather than direct depth profiling, were used to obtain diffusivities. Thus, direct comparison of bulk vs. RBS analysis for the purposes of assessing relative diffusivities of different noble gases is unwise. Minerals which do have systematically varying activation energies for the noble gases could have Arrhenius relations for the different noble gases that converge at high temperature. That is, at sufficiently high temperatures two (or more) noble gases may diffuse at the same rate independent of atomic radius or mass. The question then becomes whether such temperatures are relevant to Earth systems. Figure 9 shows where the Arrhenius relationships converge for ilmenite, quartz, and Ba-silicates. In these cases, the minimum temperature of convergence is in the range of 1150-1725 °C. Such temperatures are relevant to the mantle. Thus, based

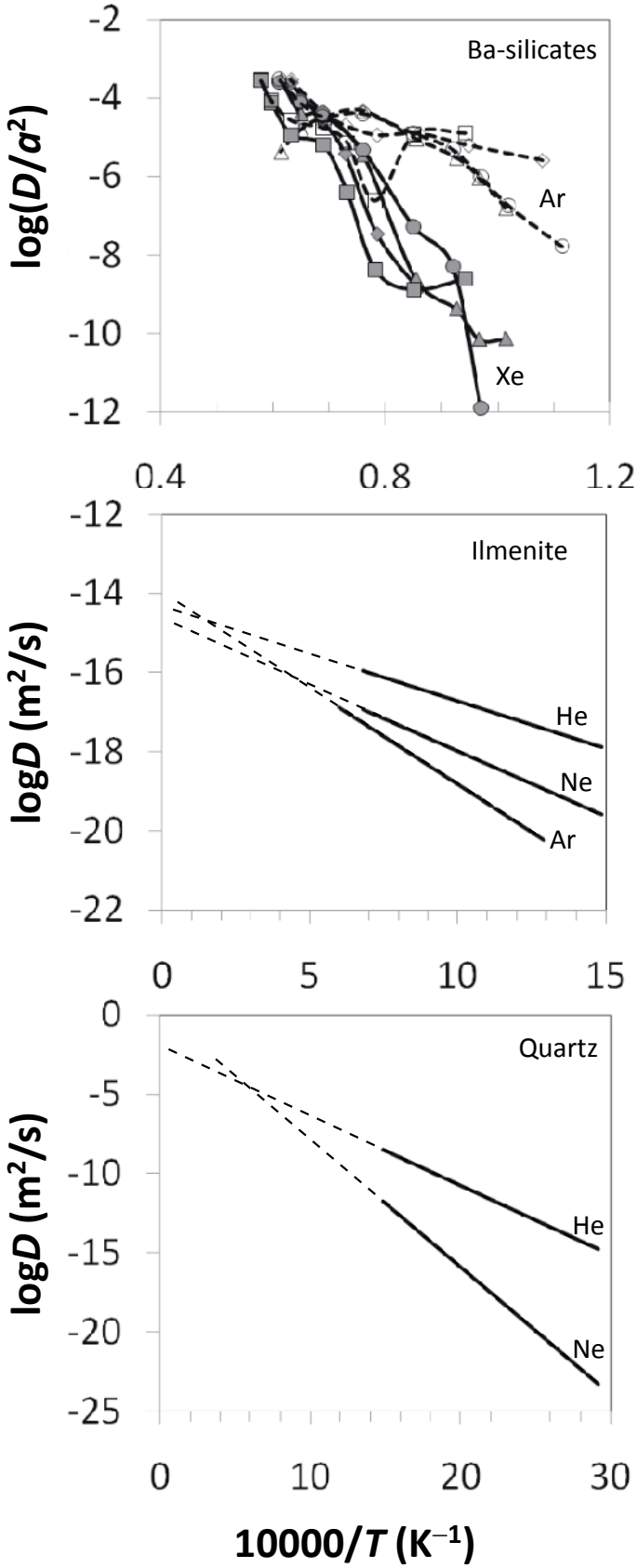

Figure 9. Minerals for which two or three noble gas diffusivities were measured in the same experimental study. A) various Ba-silicates (from Hetherington and Villa 2007). B) Ilmenite (from Futagami et al. 1993). C) quartz (from Shuster and Farley 2005). Lines (dashed = Ar; solid = Xe) linking data points of Hetherington and Villa (2007) in panel A are for clarity. Dashed lines in B and C show extrapolations to high temperatures to show if/where diffusivities of different noble gases would converge. In each case, convergence occurs at temperatures as low as ~1150 °C, ~1725 °C, ~1400 °C (for Ba-silicates, ilmenite, and quartz respectively).

on quite limited data at the current time, it appears that while noble gases indeed diffuse at dramatically different rates ($D_{He} > D_{Ne} > D_{Ar} > D_{Xe}$) in crustal and near surface temperatures, at mantle temperatures some or all noble gases may diffuse at comparable rates (if ilmenite, quartz, and Ba-silicate behavior is at all indicative of more common mantle minerals such as olivine, pyroxene, garnet, and spinel). If this observation is true and is borne out by additional high temperature (and high pressure) multiple noble gas diffusion studies, then diffusion would not be a process by which the different noble gases could be fractionated from each other in mantle minerals. It could, however, still be possible to fractionate noble gases by diffusion in melts, or by differential partitioning between melt and minerals.

CHOOSING THE "RIGHT" DIFFUSION DATA

In preparing a review of such a vast literature as has been done here, one cannot help but ask (or be asked) which of all the available studies, and which of all the available data, represents the "best" choice. In a given research project calling on a model of diffusive transport of noble gases within a particular mineral, whose diffusion data should be used? Inevitably, the answer to this question could reasonably vary depending on the particular scientific application, the pre-conceived biases of the individual scientist, and certainly during the lifetime of a scientist. On the latter point, it is surely the case that whatever recommendations are given today, those data will be superseded in the future by "better" data, buoyed by better understanding of the processes at play, better analytical methods, and better experimental methods. Generally speaking, it is therefore the case that the most recently published data, employing the most well developed (and well tested) methods, with the most direct relevance to the scientific context at hand, will be the best choice. However, this is not necessarily always the case. This problem seems particularly challenging for the noble gases given the significant analytical and experimental hurdles in their measurement and the ever-increasing complexity of their behavior in crystalline materials that is evident in each new study. Below I provide brief commentary on some of the issues that might be considered in making this choice now, and in the future, as newer data become available.

Available data make it clear that diffusion (or other) phenomena governing the transport of individual noble gas atoms through a crystalline lattice can vary depending on the scale of observation, or on the scale of interest. This could include temporal, thermal, and spatial scales. Consider Figure 10 which shows three end-member diffusion scenarios. For example, if large mineral grains have within in them smaller diffusion domains (Fig. 10c), or fast pathways (Fig. 10b), then the macroscopic bulk diffusive behavior will be quite different (in quantitative and physical treatment) than very small scale intra-domain diffusion, or (if it could somehow be isolated and directly measured) diffusion within a single fast path. Perhaps this is best evidenced by the comparisons between RBS-measured diffusion profiles (at very small spatial scales) and bulk release characteristics of minerals like feldspar or quartz. In cases where RBS (or similar microanalytical depth profiling; eg. NRA, UV-laser) diffusion results are a good match to bulk release results (for example helium in apatite, titanite, zircon, and monazite), the simplest end-member Fickian lattice diffusion is indicated (e.g., Fig. 10a). However, when RBS and bulk release data differ (for example, Ar in potassium feldspar or olivine; see Figs. 7 and 8), which one do we use? Is one of these "right" and the other "wrong"? No. Indeed, they both have relevance to natural systems, though in this case the RBS data describe a specific small scale diffusion phenomena (likely in most cases lattice diffusion) that may not be directly applicable to larger scale *bulk* diffusion in crystals, whereas the bulk loss constitutes a complicated convolution of multiple effects and geometries—including the RBS-scale lattice diffusion as well as fast paths, or multiple domains—which might be appropriate for understanding the net behavior of the specific mineral grains under study, but which may still have limitations in direct extrapolation to nature unless the details of underlying physical mechanisms and

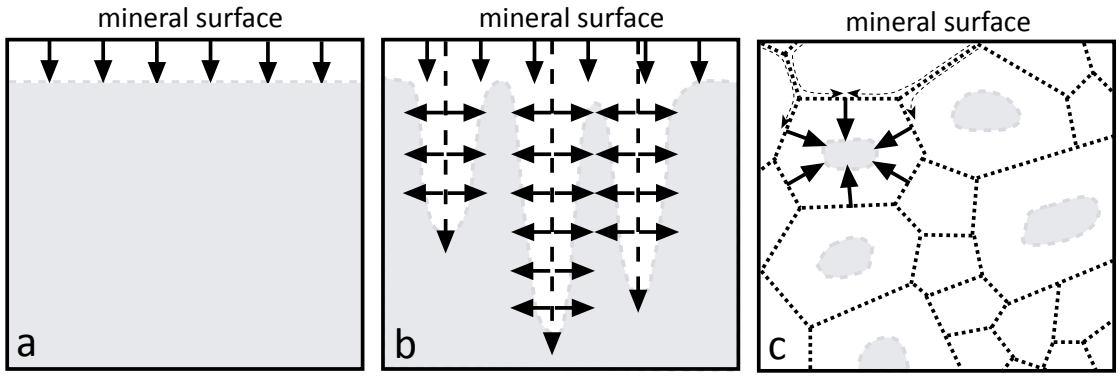

Figure 10. Cartoons showing three end-member diffusion mechanisms. Each panel represents a mineral interior with a free surface at the top into which a diffusant is penetrating (in diffusion). The gray dotted line illustrates a certain concentration contour. The gray region shows where concentrations remain below the level of the gray contour. A) simple Fickian lattice diffusion. B) Fast path diffusion. Here, lattice diffusion (solid arrows) operates from the mineral surface and also as a means of exit from the fast paths into the lattice deeper in the crystal. The fast paths (dashed arrows) have a higher (but not infinite) diffusivity than in the lattice. C) Multi-domain diffusion. Here, the mineral is divided up into multiple domains of two size classes. There is no meaning to (nor basis for) the shapes or orientations of the domains. Domains are separated by fast paths with infinite diffusivity such that all domain surfaces maintain equilibrium with the conditions at the mineral's macroscopic surface. The diffusant penetrates the mineral surface via lattice diffusion into domains cut by the surface, as well as via fast paths and into domains throughout the crystal interior. Black arrows for lattice diffusion are shown in one domain only for clarity.

structures (their precise deconvolution) could be understood to allow more general extrapolation to any natural crystal (if all the controlling parameters are known). With fast paths, the strong possibility of heterogeneous spatial distribution (or orientation) of fast paths means that at different scales of observation within a single mineral surface, different concentration vs. depth profiles, each averaging over and incorporating different proportion of fast path effects, could result (for example, consider different depth profiles into the surface of the mineral in Figure 10b or 10c taken at different locations at the surface, or with different averaging widths). At one glance, this might seem a hopeless situation wherein we might collectively throw up our arms and "give up" on the kind of diffusion modeling and interpretation which has been the mainstay of thermochronology and other diffusion-related scientific ventures for decades. This would be unwise. On the other hand, it would be equally unwise to ignore the complexities now being discovered, or to ignore the situations well known in natural systems where existing models fail. These complexities and "failures" represent opportunities to learn, datasets from which we can improve and refine our understanding of solid-state atomic transport processes, and perhaps discover new methods by which we may understand the Earth.

Table 9 has been prepared to provide a set of representative diffusion parameters for minerals most commonly used in thermochronology. In some cases, the available data are considered and averaged together (average of $\log D_0$ and E_a from each experimentally derived Arrhenius relation) as long as there is general consistency of the data and trends and no reason to reject any of the available data. These average representative values are meant to incorporate the range of diffusion data, and different analytical methods and starting materials. In these cases, the average value may be seen in comparison to the individual Arrhenius relations of the various studies in Figure 3 (titanite), Figure 4 (zircon), Figure 5 (monazite), Figure 7 (feldspar). For helium in zircon, even though Cherniak et al. (2009) found anisotropy, the *c*-perp and *c*-para relations nicely bracket the bulk release data. As their combined effects contribute to the bulk release behavior, all of these data were averaged as indicated. For potassium feldspar, only the lower temperature data of Wartho et al. (1999) along with the Foland (1974) data and the higher activation energy laser data of Clay et al. (unpub) were averaged (Fig. 7). The high

Table 9. Representative diffusivities and closure temperatures of helium and argon in commonly dated minerals.

Mineral	gas	E_a (kJ/mol)	D_0 (m^2/s)	a for T_c (μm)	geo	T_c	T_c	T_c	Reference
						1 °C/Myr	10 °C/Myr	100 °C/Myr	
Apatite	He	138	3.16E-03	75	sph	58	73	90	"best estimate" of Farley (2000)
Zircon	He	164	1.95E-05	75	cyl	167	190	215	ave of Reiners et al. (2004), Cherniak and Watson (2010)
Titanite	He	174	8.77E-04	250	sph	173	196	220	ave of Shuster et al. (2004), Cherniak and Watson (2009), Reiners and Farley (1999)
Monazite	He	202	1.25E-03	75	sph	216	239	264	ave of Cherniak and Watson (2009), Boyce et al. (2005), Farley (2007)
Plagioclase	Ar	168	1.42E-04	500	sph	189	213	240	Cassatta et al. (2009) (average)
K Feldspar	Ar	177	1.84E-07	500	sph	295	330	370	ave of Clay et al. (unpub.), Foland (1974), Wartho et al. (1999) (low-*T*)
Biotite	Ar	197	7.5E-06	500	cyl	313	347	384	McDougall and Harrison (1999)
Muscovite	Ar	264	2.3E-04	500	cyl	449	487	529	Harrison et al. (2009)
Hornblende	Ar	276	6.0E-06	500	sph	532	577	628	Harrison (1981)
Quartz	Ar	43	3.1E-19	500	sph	183	276	411	Thomas et al. (2008) & Watson and Cherniak (2003)

temperature portion of the Wartho et al. (1999) data (above their documented kink) as well as the low activation energy laser depth profile data from Clay et al. (unpub) were excluded. With potassium feldspar, here is a case where the scale of observation produces apparently different results. The fact that the bulk release data of Foland (1974) and the deeply penetrating depth profiles of Wartho et al. (1999) and Clay et al. (unpub) yield results consistent with each other and consistent with natural thermochronologic constraints is an encouraging sign that there is some direct natural relevance to these diffusivities, even if they are masking or averaging over a more complex microscale process. Precisely how bulk, deeply penetrating diffusivities are manifested in microscale potassium feldspar characteristics, which may include fast paths or multiple domains, remains unclear and an important topic for future work. In the case of apatite, I chose to use only the recommended values from Farley (2000), as they represent the most complete bulk degassing study of Durango apatite (thus, most appropriate for thermochronologic use when also employing bulk degassing analysis), but do not include the important added complexity of radiation damage effects shown in Figure 2 and discussed at length above. For all others, the most recent available data is given and/or averaged. Data for hornblende from Harrison (1981) are given as this mineral is commonly used in thermochronology, though more recent work suggests that Ar diffusion in amphibole is more complex (see above); more research is needed to better constrain Ar diffusion in amphibole.

Role of noble gas diffusion data in Ar/Ar and (U-Th)/He thermochronology

While the role of diffusion in governing the "cooling ages" recorded in minerals had been recognized and discussed earlier, it was Dodson (1973) who formulated a lasting, if not somewhat overused, analytical relationship between the diffusivity of a daughter element and the "closure temperature" for that element in that mineral grain. The so-called "Dodson Equation" has been used by students and scholars for decades to determine closure temperatures. Closure is not an instantaneous event; rather it is a gradual process that occurs within an interval in time and temperature. The Dodson closure temperature lies within that broad closure interval. The equation gives the closure temperature for a mineral given cooling rate (dT/dt), effective diffusion radius (a), and the diffusion parameters for the radiogenic isotope of interest in the mineral of interest, D_0 and E_a, as:

$$T_c = \frac{E_a / R}{\ln\left(\frac{ART_c^2(D_0/a^2)}{E_a(dT/dt)}\right)}$$

where R is the gas constant, and A is a geometric factor (27 for cylinder, 55 for sphere), and temperature is in Kelvin. What are often lost in the use of the Dodson Equation are the myriad assumptions and simplifications that must accompany its use. Among these limitations is the very real possibility, documented in some field and lab studies, that the resetting and closure of a given mineral has less to do with diffusion and more to do with fluid-induced recrystallization (i.e., a "geohygrometer" cf. Villa 2006; also see Baxter 2003b and Bosse et al. 2009). In practice, care should always be taken to evaluate (via microtextural and microchemical observation) the possibility of dissolution-precipitation reaction processes, rather than diffusion processes, influencing a given mineral or suite of minerals in age interpretation. Insofar as this chapter focuses on diffusion, the remaining treatment here will focus on the end-member situation (which seems often enough to be the case in low temperature cooling in crustal contexts) where diffusion is the primary control on radiogenic daughter retention. Some of the key assumptions embedded within the Dodson formulation that may indeed be violated in natural conditions include: monotonic cooling rate (e.g., Reiners 2009), Fickian volume diffusion (i.e., no fast paths; e.g., Lee 1995; Villa et al. 1996), simple diffusion geometry (e.g., Hourigan et al. 2005; Watson et al. 2010), homogeneous initial distribution of

daughter isotope (e.g., Boyce et al. 2005; Shuster and Farley 2004), maintenance of a zero-concentration boundary condition (e.g., Baxter et al. 2002; Baxter 2003a), cooling beginning from well above the closure temperature (e.g., Ganguly and Tirone 1999), and applicability of available constraints (typically lab-based) on D_0 and E_a to the particular mineral grain under study in nature, which may be complicated by compositional effects (e.g., Boyce et al. 2005; Farley 2007), radiation damage effects (e.g., Shuster and Farley 2009), and instability of mineral structures during certain laboratory conditions (e.g., Hetherington and Villa 2007; Villa 2010). In addition, determination of closure temperature requires identification of the lengthscale (or lengthscales) "*a*" for diffusion, which may typically be the macroscopic grain size, or, in the case of the MDD model a population of intracrystalline domains (see discussion above). For a fuller treatment of the assumptions, simplifications, and related limitations of the Dodson Equation, the reader is referred to any of the papers referenced above as well as to McDougall and Harrison (1999) and Watson et al. (2010a).

Figure 11 shows closure temperatures for several minerals of thermochronologic interest calculated with the Dodson Equation, using the representative parameters and grain sizes given in Table 9. It cannot be stressed enough that these closure temperatures will change as grain size differs, or as any of the key assumptions of the simple Dodson formulation (listed above) are violated. For example, the diffusion parameters chosen for apatite are from Farley (2000) based on the Durango apatite. Accounting for radiation damage effects (discussed above) can lead to quite significant shifts in helium closure temperature for apatite, up to tens of degrees (e.g., Shuster and Farley 2009). This figure does, however, provide a first order means of comparison of the diffusional closure properties of these minerals. Generally, He closure temperatures are much lower than Ar closure temperatures, though Ar-in-feldspar can

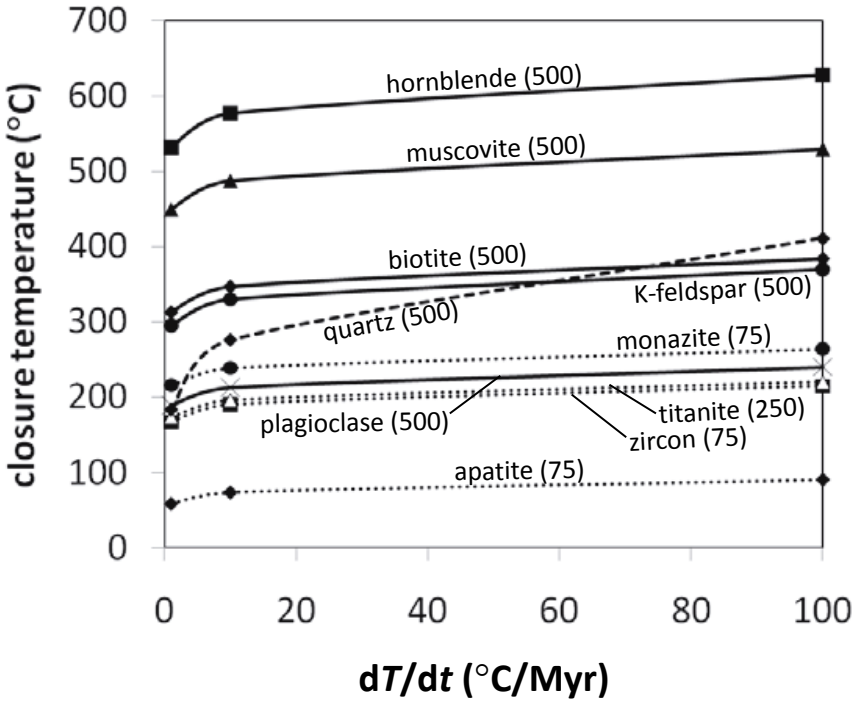

Figure 11. Closure temperatures (T_c) for commonly dated minerals. T_c calculated using the Dodson Equation (cf. Dodson 1973) for selected diffusion parameters, grain sizes, and geometries given in Table 9 for each mineral. Solid lines are for Ar closure. Dotted lines are for He closure. The dashed line is for Ar in quartz, representing a mineral with very low apparent activation energy. Grain radii (in μm) are shown in parentheses for each mineral on the plot. These representative values will change as grain size (or effective diffusion domain size) changes, or if any of the simple assumptions of the Dodson Equation (see text) do not hold.

extend to lower temperatures overlapping some of the (U-Th)/He chronometers, especially if grain size (or domain size) is smaller than that plotted. Closure of argon in quartz is also plotted because, as shown by Watson and Cherniak (2003) and Baxter (2003a), RBS measured quartz diffusivities exhibits remarkably low activation energy, which makes its effective closure quite sensitive to cooling rate. Essentially, quartz spends a great span of temperatures within a "partial retention zone" and thus is capable of taking up, or slowly leaking, excess Ar derived from its surroundings (Baxter 2003a). Insofar as the apparent solubility of Ar in quartz is enormous (Watson and Cherniak 2003), quartz has the potential to serve as a major storehouse for Ar within large portions of the crust, and even has potential as a sensitive thermochronometer based on locally derived inherited excess Ar (Baxter 2003a).

In addition, there is the possibility, raised by several studies, that diffusion is not Fickian in some minerals and may instead include the effects of "fast paths" (e.g., Lee 1995; Villa et al. 1996; Kelley et al. 2008). Generally, fast path diffusion will have the effect of shortening the effective lattice diffusional radius and provide faster (though not necessarily infinitely fast) transport through the mineral. Fast paths should in general result in lower closure temperatures. An end-member case of "fast-paths" is the MDD-model where the fast paths bounding the domains do have infinite diffusivity; in this case the behavior is simple Fickian lattice diffusion with the key complexity being the identification and assignment of intra-domain sizes and distributions. When the fast path diffusion is faster than the lattice diffusion, but not so much so that it can be treated as infinite, then fast-path diffusion becomes relevant and complicated. Interestingly, as shown in Figure 12, if the activation energies of fast path diffusion and lattice diffusion differ significantly (indeed as shown by potassium feldspar and olivine, Figs. 7 and 8, respectively) then such a mineral may experience MDD-like behavior

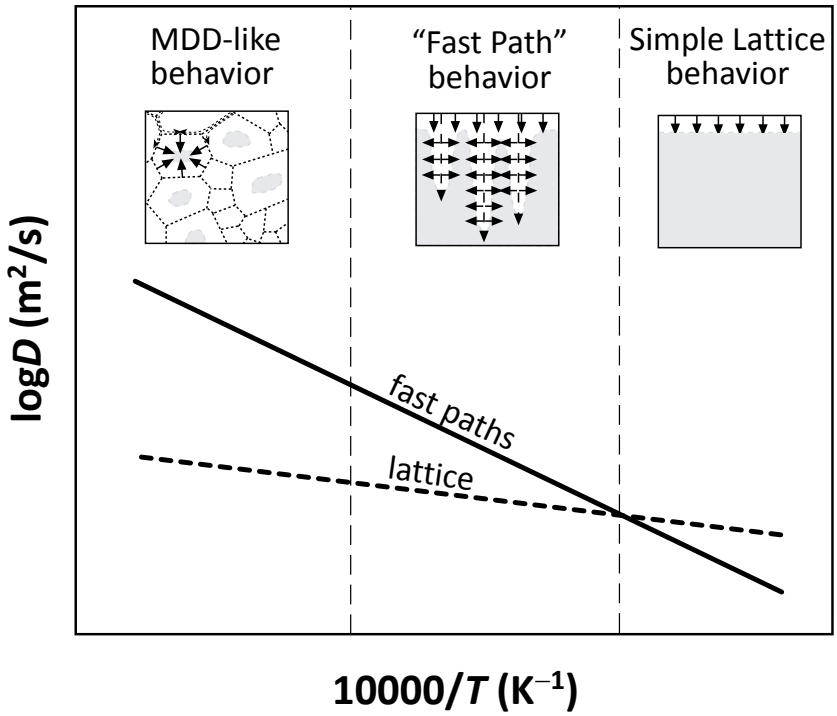

Figure 12. Cartoon Arrhenius relations for hypothetical lattice diffusion (dashed) and fast path diffusion (solid) within a single mineral showing the evolving role of fast paths and lattice diffusion with temperature. Given the higher activation energy for fast paths than lattice diffusion, at high temperatures diffusion in the fast paths may be treated as effectively infinite and the bulk behavior will be MDD-like (i.e., Fig. 10c). At intermediate temperatures, diffusion in the fast paths is still faster than in the lattice, but not infinitely so, thus their complex interactions must be treated via a fast path model (i.e., Fig. 10b). At low enough temperatures, the lattice and fast path lines cross over and only simple lattice diffusion is relevant (i.e., Fig. 10a).

(at the highest temperatures where fast path diffusion is much faster than lattice diffusion) *and* fast-path diffusion behavior (at intermediate temperatures where fast path diffusion is only somewhat faster than lattice diffusion) *and* simple lattice diffusion behavior (at lowest temperatures when lattice diffusion is actually faster than in the no-longer-aptly-named "fast paths") as the temperature of the system evolves and the relative diffusivities of the lattice and fast paths changes. In such a case, the question then becomes which of these situations is relevant for natural temperatures and timescales. The apparent convergence of lattice (low activation energy) and fast path (high activation energy) diffusivity within potassium feldspar (Fig. 7) and olivine (Fig. 8), as well as its possible relevance to MDD (e.g., Lovera et al. 1989) or fast path (e.g., Lee 1995) modeling, is therefore significant and merits further study. In this context, it is important to bear in mind that the fast path phenomena (shown in Figs. 6, 7, and 12) represent the convolution of the actual fast path diffusion and the accompanying lattice diffusivity into and out of the fast paths as indicated in the Figure 10b cartoon. It is interesting as well that the fast diffusion pathways identified here have markedly higher activation energies than related lattice diffusivities. Why this should be the case is unclear, though Zhang et al. (2006, and references therein) offers some discussion of this including the possibility that impurity segregation may increase fast path E_a. Fast path diffusion is difficult to model, especially given that we still have very little constraint on the exact identity and geometry of the purported fast paths. In addition to fast path modeling efforts such as Lee (1995) or Zhang et al. (2006) and references therein, the thermochronological community might benefit from consideration of the modeling efforts that exist in the broadly similar context of grain boundary diffusion. Grain boundaries are *not* the same as "fast paths" within minerals, but insofar as both grain boundaries and "fast paths" represent short circuit pathways surrounded by the normal mineral lattice (with slower diffusivity), some general lessons might cautiously be gained in the comparison as efforts to understand and model fast path diffusion in thermochronology continue. For further discussion of grain boundary diffusion the reader is referred to Dohmen and Milke (2010) and references therein.

SUGGESTIONS FOR FUTURE STUDY

In this chapter, several active and future areas of research have been discussed in detail, or in passing. In closing, it is worth summarizing some of the key issues and that may help direct the study of noble gas diffusion.

Diffusion at high pressures and temperatures

There are essentially no data on noble gas diffusion at high pressures (greater than 100-200 MPa) appropriate for the deep Earth or other planetary interiors. A few reports on micas by Harrison et al. (2009) and McDougall and Harrison (1999) show a ~14 cm^3/mol activation volume, enough to lead to significant pressure effects, especially within the mantle adiabat where the counteracting effects of increasing temperature on diffusion are small (Watson and Baxter 2007). New experimental approaches, along the lines of those developed by Parman et al. (2009) will be required to overcome the dearth of high pressure diffusion data for more important mantle minerals such as olivine, pyroxene, and garnet.

Diffusion of Ar and He in common mantle minerals

In general, modern diffusion data for He and Ar in the most common mantle minerals are quite limited (Fig. 13), and as mentioned above none of the scant existing data are for mantle pressures. As interests evolve in the degassing history of the Earth, the lengthscales of heterogeneity of noble gas distribution within the mantle, and the preservation of such heterogeneities over time, robust quantification of noble gas diffusivities in mantle minerals will be of value (e.g., Parman et al. 2005; Baxter et al. 2007; Hart et al. 2008; Thomas et al. 2008; Jackson et al. 2009; Kurz et al. 2009). The available data for He, for example, show roughly

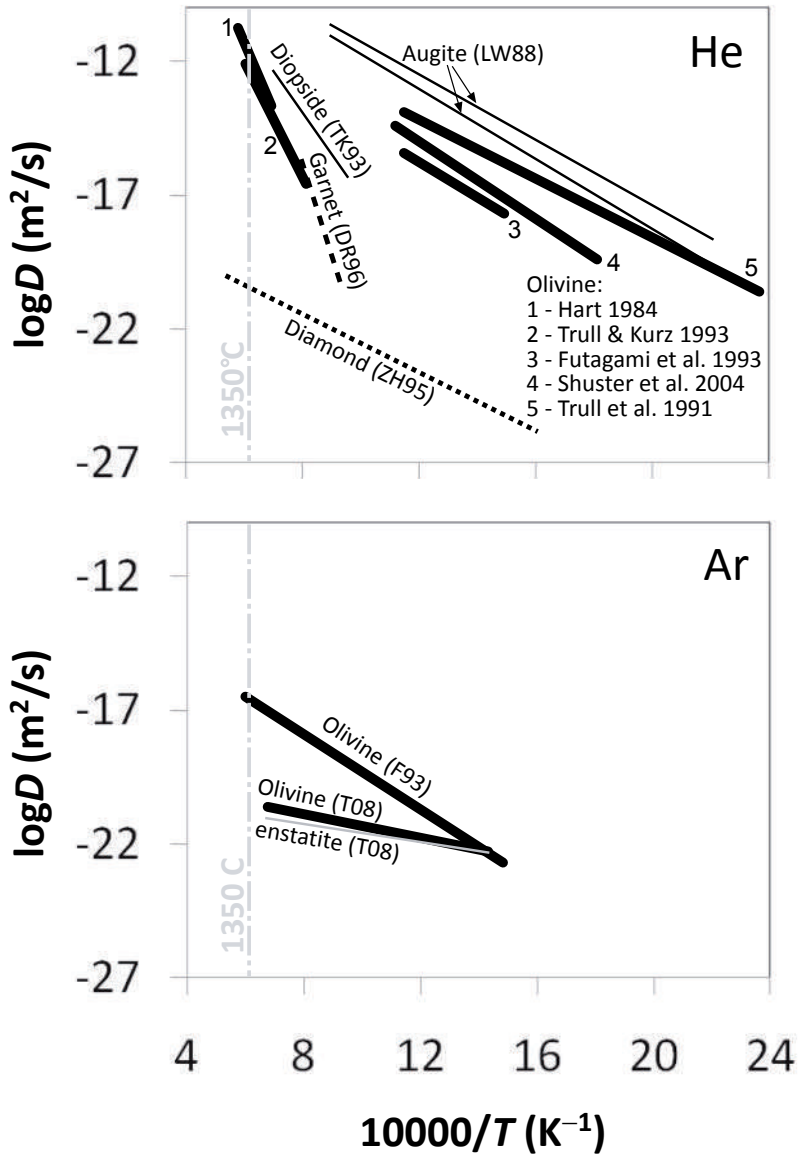

Figure 13. Diffusion of He (A) and Ar (B) in common mantle minerals. Labeled lines derive from the following sources: LW88 - Lippolt and Weigel (1988); TK93 - Trull and Kurz (1993); DR96 - Dunai and Roseleib (1996); ZH95 - Zashu and Hiyagon (1995); F93 - Futagami et al. (1993); T08 - Thomas et al. (2008). References for olivine data are numbered and given in the figure. There are surprisingly little data and important inconsistencies between studies exist (e.g., olivine activation energies).

converging diffusivities at mantle temperatures (~1350 °C) but the activation energies from different studies vary widely. The studies of Hart (1984) and Trull and Kurz (1993) for olivine as well as Trull and Kurz (1993) for pyroxene and Dunai and Roselieb (1996) for garnet indicate the highest activation energies (502, 420, 290, 660 kJ/mol, respectively) of any noble gas in any mineral reported in the literature (earlier studies of He and Ar diffusion in diamond reported even higher E_a, but were likely compromised by graphitization or other effects; see Zashu and Hiyagon 1995). No other published study of He or Ar in any mineral (except an early study of He and Ar diffusion in beryl by Toyota and Ozima 1988 where scattered data may have been compromised by heterogeneous noble gas distribution) indicates E_a greater than 276 kJ/mol (see all Tables). These studies (on dense nesosilicates as well as pyroxene at high temperatures of 770-1460 °C) yielding high E_a thus stand as notable outliers in comparison to other data. Trull and Kurz (1993) suggest that there may be an experimental artifact related to fast paths and/

or to helium trapped in CO_2 rich gas inclusions within olivine samples yielding high activation energies. In contrast, the studies of Lippolt and Weigel (1988), Trull et al. (1991), Futagami et al. (1993), and Shuster et al. (2004) indicate much lower activation energies for helium diffusion in olivine and pyroxene, though these studies spanned lower temperatures of 150-850 °C (see Fig. 13 and Table 5). Hart et al. (2008) suggest that studies yielding lower activation energies and higher diffusivities for helium in olivine at low temperatures (specifically citing Trull et al. 1991 and Shuster et al. 2004) might suffer from radiation damage effects, though Shuster et al. (2004) show that proton-bombardment (used to produce ^{3}He in their olivine samples) did not create radiation damage effects in apatite and titanite (unlike *neutron* irradiation which *does* produce radiation damage effects; e.g., Shuster and Farley 2009). In any case, the radiation damage studies of Shuster et al. (2006) and Shuster and Farley (2005, 2009) indicate that the addition of finite radiation damage serves to *decrease* (not increase) the diffusivity of helium in apatite and quartz. As long as the *relative* effects of radiation damage documented in these studies on apatite, titanite and quartz may be extended and applied to olivine (although this has yet to be demonstrated) then radiation damage cannot be invoked to discount the low activation energy diffusion data for olivine (e.g., Trull et al. 1991; Futagami et al. 1993; Shuster et al. 2004). Lastly, it is also possible that the diffusion mechanism (and Arrhenius relations) for helium in these mantle minerals simply changes somewhere between low (150-850 °C) and high (770-1460 °C) temperatures which could reconcile the high and low E_a data for helium reviewed here. However, data from an unpublished step-heating experiment on proton-bombardment induced ^{3}He in San Carlos olivine shows a robust linear Arrhenius relationship spanning 400 to 1125 °C with activation energy ~166 kJ/mol (DL Shuster, personal communication), slightly higher than the Shuster et al. (2004) and Trull et al. (1991) results (140 and 105 kJ/mol, respectively), but still significantly lower than the activation energies reported by Hart (1984) and Trull and Kurz (1993) (502 and 420 kJ/mol, respectively). Thus, if there is a "kink" in the Arrhenius relationship for helium diffusion in olivine, it has yet to be documented within a single study. Fortunately, the available diffusion data for helium in olivine appear to converge at upper mantle temperatures (i.e., around 1350 °C; Fig. 13) but extrapolation to higher (or lower) temperatures is uncertain given the current data. At present, the Shuster et al. (2004) data seems most robust given that the helium was implanted uniformly via proton bombardment (probably with no significant radiation damage effects), which should eliminate potential problems associated with gas inclusions or heterogeneous noble gas distribution that Trull and Kurz (1993) described. Clearly, uncertainties in helium diffusivity in mantle minerals remain to be resolved.

Currently very little data on Ar diffusion in mantle minerals exists. Futagami et al. (1993) report an activation energy for Ar diffusion in olivine of 134 kJ/mol. A recent abstract by Cassata and Renne (2010) reports the results of ^{37}Ar diffusion experiments in gem-quality pyroxene yielding much higher activation energies > 300 kJ/mol. Finally, the data of Thomas et al. (2008) for argon diffusion in olivine and pyroxene, using RBS depth profiling, indicate the lowest activation energies (42-32 kJ/mol) that they interpret to reflect the influence of trapping by isolated point defects. This large disparity in apparent activation energies for Ar in mantle minerals remains unresolved. Whether any of these data can be extrapolated as a bulk property of mantle minerals, or whether olivine and pyroxene (similar to potassium feldspar) might be characterized by bulk fast path behavior to enhance bulk diffusivity, is an important topic worthy of continued study. The diffusivity of noble gases in mantle minerals has been used to estimate lengthscales of diffusive transport within the mantle (e.g., Hart et al. 2008), but in a bulk rock system the diffusion via wetted or dry grain boundaries between crystals (e.g., Baxter et al. 2007), or via fast paths that may exist within crystals, should also be considered as new data for grain boundaries and fast paths emerge. The possibility that the diffusivities of multiple noble gases may actually converge at mantle temperatures as suggested above (Fig. 9) is also worth testing.

In situ depth profile analysis

Recent work employing RBS, NRA or laser depth profiling allows submicrometer scale distribution patterns of noble gases to be determined directly. Insofar as those distributions reflect diffusive uptake or loss (natural or experimental) this information is a critical complement to bulk diffusion and/or step heating experiments. Especially as the recent RBS and 193-nm laser studies of Ar diffusion seem to be showing a fundamentally different pathway than bulk release data, there is much to be learned by integrating and reconciling these different datasets and modes and scales of observation. The advances will be made when multiple methods of observation are employed in concert.

Quantification of noble gas diffusion within "fast paths"

On the basis of the complex diffusive behavior of noble gases in many minerals, the role of "fast paths" has been hypothesized and modeled in several contexts (e.g., Lee 1995). Still, the physical identity of a fast path remains uncertain as is the actual diffusivity and holding capacity of the fast path. The net diffusive flux via fast paths is determined both by the molecular diffusivity of an atom residing therein, and, on the capacity (i.e., partitioning) of the fast path feature to hold atoms with respect to the surrounding "normal" lattice of the host phase (e.g., Watson and Baxter 2007). As discussed above, an admittedly imperfect analogy may be drawn here to grain boundary diffusion, insofar as grain boundaries represent fast paths within a polycrystalline aggregate (Dohmen and Milke 2010). Experiments on polycrystalline diopside aggregates by Baxter et al. (2007) showed that significant amounts of He and Ar could partition into grain boundaries between minerals. However, as of yet, there are no grain boundary diffusion data for the noble gases (e.g., Dohmen and Milke 2010). Until combined analytical and observational techniques are developed to identify and isolate fast path features within minerals, improved quantification of fast path diffusion and fast path storage capacity will be extremely difficult.

Integrated studies with multiple noble gases

When preparing this chapter, this author was surprised at the extremely scant literature on multiple noble gases within single studies. As shown, for example, by Hetherington and Villa (2007), valuable information about mechanisms of gas release can be gained by comparing the diffusive (or release) behavior of multiple noble gases. Such studies might be best accomplished by exploiting irradiated samples wherein isotopes of more than one noble gas are produced (e.g., Shuster and Farley 2005; Hetherington and Villa 2007) or mixed gas in-diffusion experiments wherein more than one noble gas may be introduced.

Quantification of effects of radiation damage, defects, and deformation

Based on the available data, it is clear that imperfections in mineral structures—whether induced by radioactive decay damage, mechanical deformation, or "fast paths"—can cause major changes in noble gas diffusion and retentivity. Many questions remain as to the exact physical nature of these structural defects and their origins, and even if and when such damage serves to increase, or decrease, apparent diffusivity. Unexplained differences between synthetic and natural minerals remain as do the underlying reasons for the differing effects of various types of radiation damage (e.g., proton-bombardment vs. neutron irradiation vs. alpha recoil vs. spontaneous fission). It is also not yet clear the extent to which lessons learned about the damage effects within one mineral (e.g., apatite) may be extrapolated to other minerals experiencing similar radiation or other structural damage. Combination of existing noble gas analytical approaches with SEM or TEM scale observations of damaged, deformed, or imperfect minerals may permit the development and refinement of quantitative models (like the RDAAM model of Flowers et al. 2009) to account for and model these effects.

ACKNOWLEDGMENTS

The author wishes to thank P.L. Clay, S.P. Kelley, E.B. Watson, J.B. Thomas, D.J. Cherniak, P.D. Asimow, K.A. Farley, D.J. DePaolo and P.R. Renne for collaborations and numerous discussions including many of the themes in this chapter over that past decade. D.L. Shuster and I.M. Villa provided valuable informal commentary and discussion based on an early draft of this chapter and M.T. Heizler, D.J. Cherniak, & Y. Zhang provided formal reviews and editing all of which helped to improve the chapter. NSF EAR-0337527 to EFB supported much of the foundational work which made the writing of this chapter possible.

REFERENCES

Aciego S, Kennedy BM, DePaolo DJ, Christensen JN, Hutcheon I (2003) Reply to comment on "U-Th/He age of phenocrystic garnet from the 79AD eruption of Mt Vesuvius." Earth Planet Sci Lett 250:404-405

Aciego S, Kennedy BM, DePaolo DJ, Christensen JN, Hutcheon I (2006) (U-Th)/He age of phenocrystic garnet from the 79 AD eruption of Mt. Vesuvius. Earth Planet Sci Lett 216:209-219

Bahr R, Lippolt HJ, Wernicke RS (1994) Temperature-induced ^{4}He degassing of specularite and botryoidal hematite: a ^{4}He retentivity study. J Geophys Res 99:17695-17707

Baldwin SL, Harrison TM, Fitz Gerald JD (1990) Diffusion of ^{40}Ar in metamorphic hornblende. Contrib Mineral Petrol 105:691-703

Ballentine CJ, Burnard PG (2002) Production, release and transport of noble gases in the continental crust. Rev Mineral Geochem 47:481-538

Baxter EF (2003a) Quantification of the factors controlling the presence of excess Ar or He. Earth Planet Sci Lett 216:619-634 [Note: the reader should refer to p. 449 of Baxter et al. 2007 to find a correction to the key equation in this paper.]

Baxter EF (2003b) Natural constraints on metamorphic reaction rates. Geol Soc Lond Spec Pub 220:183-202

Baxter EF, Asimow PD, Farley KA (2007) Grain boundary partitioning of Ar and He. Geochim Cosmochim Acta 71:434-451

Baxter EF, Clay PL, Kelley SP, Watson EB, Thomas J, Cherniak DP (2006) Two diffusive pathways for quartz and feldspar. Geochim Cosmochim Acta 70:A41

Baxter EF, DePaolo DJ, Renne PR (2002) Spatially Correlated Anomalous ^{40}Ar/^{39}Ar "Age" Variations About a Lithologic Contact near Simplon Pass, Switzerland: A Mechanistic Explanation for Excess Ar. Geochim Cosmochim Acta 66:1067-1083

Behrens H (2010) Noble gas diffusion in silicate glasses and melts. Rev Mineral Geochem 72:227-267

Blackburn TJ, Stockli DF (2006) Comment on "U-Th/He age of phenocrystic garnet from the 79 AD eruption of Mt. Vesuvius" by Sarah Aciego, B.M. Kennedy, Donald J. DePaolo, John N. Christensen, and Ian Hutcheon [Earth Planet Sci Lett 216 (2003) 209-219]. Earth Planet Sci Lett 250:402-403

Blackburn TJ, Stockli DF, Walker D (2007) Magnetite (U-Th)/He dating and its application to the geochronology of intermediate to mafic volcanic rocks. Earth Planet Sci Lett 259:360-371

Blard P-H, Puchol N, Farley KA (2008) Constraints on the loss of matrix-sited helium during vacuum crushing of mafic phenocrysts. Geochim Cosmochim Acta 72:3788-3803

Bosse V, Boulvais P, Gautier P, Tiepolo M, Ruffet G, Devidal JL, Cherneva Z, Gerdjikov I, Paquette JL (2009) Fluid-induced disturbance of the monazite Th-Pb chronometer: *In situ* dating and element mapping in pegmatites from the Rhodope (Greece, Bulgaria). Chem Geol 261:286-302

Boyce JW, Hodges KV (2005) U and Th zoning in Cerro de Mercado (Durango, Mexico) fluorapatite: Insights regarding the impact of recoil redistribution of radiogenic ^{4}He on (U-Th)/He thermochronology. Chem Geol 219:261-274

Boyce JW, Hodges KV, King D, Crowley JL, Jercinovic M, Chatterjee N, Bowring SA, Searle M (2009) Improved confidence in (U-Th)/He thermochronology using the laser microprobe: an example from a Pleistocene leucogranite, Nanga Parbat, Pakistan. Geochem Geophys Geosystems 10:Q0AA01

Boyce JW, Hodges KV, Olszewski WL, Jercinovic MJ (2005) He diffusion in monazite: implications for (U-Th)/He thermochronology. Geochem Geophys Geosystems 6:Q12004

Burkland MK, Swindle TD, Baldwin SL (1995) Isothermal heating experiments on Bjurbole: implications for the release mechanisms of radiogenic ^{129}Xe. Geochim Cosmochim Acta 59:2085-2094

Cassata WS, Renne PR (2010) ^{37}Ar diffusion in pyroxene: Implications for thermochronometry and mantle degassing. Geochim Cosmochim Acta 74:A148

Cassata WS, Renne PR, Shuster DL (2009) Argon diffusion in plagioclase and implications for thermochronometry: A case study from the Bushveld Complex, South Africa. Geochim Cosmochim Acta 73:6600-6612

Cherniak DJ (1993) Lead diffusion in titanite and preliminary results on the effects of radiation damage on Pb transport. Chem Geol 110:177-194
Cherniak DJ (2010) Diffusion in accessory minerals: zircon, titanite, apatite, monazite and xenotime. Rev Mineral Geochem 72:827-870
Cherniak DJ, Dimanov A (2010) Diffusion in pyroxene, mica and amphibole. Rev Mineral Geochem 72:641-690
Cherniak DJ, Lanford WA, Ryerson FJ (1991) Lead diffusion in apatite and zircon using ion-implantation and Rutherford backscattering techniques. Geochim Cosmochim Acta 55:1663-1673
Cherniak DJ, Ryerson FJ (1993) A study of strontium diffusion in apatite using Rutherford backscattering spectroscopy and ion-implantation. Geochim Cosmochim Acta 57:4653-4662
Cherniak DJ, Watson EB (2001) Pb diffusion in zircon. Chem Geol 172:5-24
Cherniak DJ, Watson EB (2009) The Fast and the Slow, the High and the Low - Investigations of Pb and He diffusion in Accessory Minerals and Implications for Geochronology. AGU Fall Meeting
Cherniak DJ, Watson EB (2010) Helium diffusion in accessory minerals. Geochim Cosmochim Acta 74:A173
Cherniak DJ, Watson EB, Thomas JB (2009) Diffusion of helium in zircon and apatite. Chem Geol 268:155-166
Clay PL, Baxter EF, Kelley SP, Watson EB, Thomas J, Cherniak DJ (2006). Multi-path diffusion: Implications for the measurement of Ar solubility and partitioning between quartz and feldspar. AGU Fall Meeting Abstract
Clay PL, Baxter EF, Cherniak DJ, Kelley SP, Thomas JB, Watson EB (2010) Two diffusion pathways in quartz: a combined UV-laser and RBS study. Geochim Cosmochim Acta 74:5906-5925
Copeland P, Harrison TM, Le Fort P (1996) Reply to the Comment on "Age and cooling history of the Manaslu granite: implications for Himalayan tectonics" by Igor Villa. J Volc Geotherm Res 70:262-264
Copeland P, Watson EB, Urizar SC, Patterson D, Lapen TJ (2007) Alpha thermochronometry of carbonates. Geochim Cosmochim Acta 71:4488-4511
Crank J (1975) The Mathematics of Diffusion, 2nd edition. Clarendon Press, Oxford
Dahl PS (1996a). The crystal-chemical basis for Ar retention in micas: Inferences from interlayer partitioning and implications for geochronology. Contrib Mineral Petrol 123:22-39
Dahl PS (1996b) The effects of composition on retentivity of Ar and O in hornblende and related amphiboles: a field-tested empirical model. Geochim Cosmochim Acta 60:3687-3700
Damon PE, Kulp JL (1957) Determination of radiogenic helium in zircon by stable isotope dilution technique. Trans Am Geophys Union 38:945-953
Dodson MH (1973) closure temperature in cooling geochronological and petrological systems. Contrib Mineral Petrol 40:259-274
Dohmen R, Milke R (2010) Diffusion in polycrystalline materials: grain boundaries, mathematical models, and experimental data. Rev Mineral Geochem 72:921-970
Dunai TJ, Roselieb K (1996) Sorption and diffusion of helium in garnet: implications for volatile tracing and dating. Earth Planet Sci Lett 139:411-421
Dunlap WJ, Kronenberg AK (2001) Argon less during deformation of micas: constraints from laboratory deformation experiments. Contrib Mineral Petrol 141:174-185
Farley KA (2000) Helium diffusion from apatite: general behavior as illustrated by Durango fluorapatite. J Geophys Res 105:2903-2914
Farley KA (2007) He diffusion systematics in minerals: Evidence from synthetic monazite and zircon structure phosphates. Geochim Cosmochim Acta 71:4015-4024
Farley KA, Reiners PW, Nenow V (1999) An apparatus for high precision helium diffusion measurements from minerals. Anal Chem 71:2059-2061
Farley KA, Stockli DF (2002) (U-Th/He) dating of phosphates: apatite, monazite, xenotime. Rev Mineral Geochem 48:559-577
Farver JR (2010) Oxygen and hydrogen diffusion in minerals. Rev Mineral Geochem 72:447-507
Fechtig H, Kalbitzer S (1966) The diffusion of argon in potassium bearing solids. *In:* Potassium - Argon Dating. Schaeffer OA, Zahringer J (eds) Heidelberg, Springer, p. 68-106
Fick A (1855) Ueber diffusion. Ann Phys Chem 94:59-86
Flowers RM (2009) Exploiting radiation damage control on apatite (U-Th)/He dates in cratonic regions. Earth Planet Sci Lett 277:148-155
Flowers RM, Ketcham RA, Shuster DL, Farley KA (2009) Apatite (U-Th)/He thermochronometry using a radiation damage accumulation and annealing model. Geochim Cosmochim Acta 73:2347-2365
Flowers RM, Shuster DL, Wernicke BP, Farley KA (2007) Radiation damage control on apatite (U-Th)/He dates from the Grand Canyon region, Colorado Plateau. Geology 35:447-450
Foland KA (1974) Ar^{40} diffusion in homogeneous orthoclase and an interpretation of Ar diffusion in Potassium feldspars. Geochim Cosmochim Acta 38:151-166
Fortier SM, Giletti B (1989) An empirical model for predicting diffusion coefficients in silicate minerals. Science 245:1481-1484

Futagami T, Ozima M, Nagai S, Aoki Y (1993) Experiments on thermal release of implanted noble gases from minerals and their implications for noble gases in lunar soil grains. Geochim Cosmochim Acta 57:3177-3194

Ganguly J, Tirone M (1999) Diffusion closure temperature and age of a mineral with arbitrary extent of diffusion: theoretical formulation and applications. Earth Planet Sci Lett 170:131-140

Gautheron C, Tassan-Got L, Barbarand J, Pagel M (2009) Effect of alpha-damage annealing on apatite (U-Th)/He thermochronology. Chem Geol 266:166-179

Gautheron CE, Tassan-Got L, Farley KA (2006) (U-Th)/Ne chronometry. Earth Planet Sci Lett 243:520-535

Giletti B (1974) Studies in diffusion. 1: Ar in phlogopite mica. *In*: Geochemical Transport and Kinetics. Hofmann A, Gilleti BJ, Yoder HS Jr., Yund RA (eds) Carnegie Institute of Washington Publ., p 107-115

Grove M, Harrison TM (1996) ^{40}Ar* diffusion in Fe-rich biotite. Am Mineral 81:940-951

Hames WE, Bowring SA (1994) An empirical evaluation of the argon diffusion geometry in muscovite. Earth Planet Sci Lett 124:161-167

Hames WE, Hodges KV (1993) Laser ^{40}Ar/^{39}Ar evaluation of slow cooling and episodic loss of ^{40}Ar from a samples of polymetamorphic muscovite. Science 261:1721-1723

Harrison C, Barry T, Turner G (2004) Possible diffusive fractionation of helium isotopes in olivine and clinopyroxene phenocrysts. Eur J Mineral 16:213-220

Harrison TM (1981) Diffusion of ^{40}Ar/^{39}Ar in hornblende. Contrib Mineral Petrol 78:324-331

Harrison TM, Celerier J, Aikman AB, Hermann J, Heizler MT (2009) Diffusion of ^{40}Ar in muscovite. Geochim Cosmochim Acta 73:1039-1051

Harrison TM, Duncan I, McDougall I (1985) Diffusion of ^{40}Ar in biotite: temperature, pressure and compositional effects. Geochim Cosmochim Acta 49:2461-2468

Hart SR (1984) He diffusion in olivine. Earth Planet Sci Lett 70:297-302

Hart SR, Kurz MD, Wang Z (2008) Scale length of mantle heterogeneities: Constraints from helium diffusion. Earth Planet Sci Lett 269:508-517

Heizler MT, Harrison TM (1998) The thermal history of the New York basement determined from ^{40}Ar/^{39}Ar Potassium feldspar studies. J Geophys Res 103:29795-29814

Heizler MT, Parsons I, Sanders RE, Heizler LL (2008) K-feldspar microtexture and argon transport. Geol Soc Am Abstracts Programs 40(6):310

Heizler MT, Ralser S, Karlstrom, KE (1997) Late Proterozoic (Grenville?) deformation in central New Mexico determined from single-crystal muscovite ^{40}Ar/^{39}Ar age spectra. Precambian Res 84:1-15

Hess JC, Lippolt HJ, Gurbanov AG, Michalski I (1993) The cooling history of the late Pliocene Eldzhurtinskiy granite (Caucasus, Russia) and the thermochronological potential of grain-size/age relationships. Earth Planet Sci Lett 117:393-406

Hetherington CJ, Villa IM (2007) Barium silicates of the Berisal Complex, Switzerland: A study in geochronology and rare-gas release systematic. Geochim Cosmochim Acta 71:3336-3347

Hiyagon H (1994) Retention of solar helium and neon in IDPs in deep sea sediment. Science 263:1257-1259

Hodges KV, Bowring SA (1995) ^{40}Ar/^{39}Ar thermochronology of isotopically zoned micas: Insights from the southwestern USA Proterozoic orogen. Geochim Cosmochim Acta 59:3205-3220

Hodges KV, Hames WE, Bowring SA (1994) ^{40}Ar/^{39}Ar age gradients in micas from a high-temperature-low-pressure metamorphic terrain: evidence for very slow cooling and implications for the interpretation of age spectra. Geology 22:55-58

Hohenberg CM, Pravdivtseva OV, Meshik AP (2004) Trapped Xe and I-Xe ages in aqueously altered CV3 meteorites. Geochim Cosmochim Acta 68:4745-4763

Honda M, Reynolds JH, Roedder E, Epstein E (1987) Noble gases in diamonds: occurrence of solar helium and neon. J Geophys Res 92:12507-12521

Hourigan JK, Reiners PW, Brandon MT (2005) U-Th zonation-dependent alpha-ejection in (U-Th)/He chronometry. Geochim Cosmochim Acta 69:3349-3365

Hyodo H, York D (1993) The discovery and significance of a fossilized radiogenic agon wave (argonami) in the Earth's crust. Geophys Res Lett 20:61-64

Jackson MG, Kurz MD, Hart, SR (2009) Helium and neon isotopes in phenocrysts from Samoan lavas: Evidence for heterogeneity in the terrestrial high ^{3}He/^{4}He mantle. Earth Planet Sci Lett 287:519-528

Kelley (2002) K-Ar and Ar-Ar Dating. Rev Mineral Geochem 47:785-818

Kelley SP, Baxter EF, Cherniak D, Clay PL, Thomas J, Watson EB (2008) Two diffusion mechanisms for argon in Potassium feldspar? Geochim Cosmochim Acta 72:A460

Kelley SP, Reddy SM, Maddock R (1994) Laser-probe ^{40}Ar/^{39}Ar investigation of a pseudotachylite and its host from the Outer Isles thrust, Scotland. Geology 22:443-446

Kramar N, Cosca MA, Hunziker JC (2001) Heterogeneous ^{40}Ar* distributions in naturally deformed muscovite: *in situ* UV-laser ablation evidence for microstructurally controlled diffusion. Earth Planet Sci Lett 192:377-388

Kurz MD, Warren JM, Curtice J (2009) Mantle deformation and noble gases: Helium and neon in oceanic mylonites. Chem Geol 266:10-18
Lee JKW (1993) The argon release mechanisms of hornblende in vacuo. Chem Geol 106:133-170
Lee JKW (1995) Multipath diffusion in geochronology. Contrib Mineral Petrol 120:60-82
Lee JKW (2009) Using argon as a temporal tracer of large-scale geologic processes. Chem Geol 266:104-112
Lippolt HJ, Leitz M, Wernicke RS, Hagedorn B (1994) (Uranium + thorium)/helium dating of apatite: experience with samples from different geochemical environments. Chem Geol 112:179-191
Lippolt HJ, Weigel E (1988) ^{4}He diffusion in ^{40}Ar retentive minerals. Geochim Cosmochim Acta 52:1449-1458
Lovera OM, Grove M, Harrison T (2002) Systematic analysis of potassium feldspar ^{40}Ar/^{39}Ar step heating results II: relevance of laboratory argon diffusion properties to nature. Geochim Cosmochim Acta 66:1237-1255
Lovera OM, Grove M, Harrison TM, Mahon KI (1997) Systematic analysis of Potassium feldspar ^{40}Ar/^{39}Ar heating results: I. Significance of activation energy determinations. Geochim Cosmochim Acta 61:3171-3192
Lovera OM, Harrison TM, Grove M (1996) Comment on "Multipath Ar transport in K-feldspar deduced from isothermal heating experiments" by Igor Villa. Earth Planet Sci Lett 140:281-283
Lovera OM, Richter FM, Harrison TM (1989) The ^{40}Ar/^{39}Ar thermochronometry for slowly cooled samples having a distribution of diffusion domain sizes. J Geophys Res 94:17917-17935
McDougall I, Harrison TM (1999) Geochronology and Thermochronology by the 40Ar/39Ar Method. Oxford University Press
McLaren S, Dunlap WJ, Powell R (2007) Understanding potassium feldspar ^{40}Ar/^{39}Ar data: reconciling models, methods, and microtextures. J Geol Soc 164:941-944
Melcher CL, Burnett DS, Tombrello TA (1981) Xenon diffusion following ion implantation into feldspar: Dependence on implantation dose. Proc Lunar Planet Sci I2B:1725-1736
Melcher CL, Tombrello TA, Burnett DS (1983) Retention of ion-implanted-xenon in olivine: dependence on implantation dose. Geochim Cosmochim Acta 47:1707-1712
Mulch A, Cosca MA, Handy MR (2002) *In situ* UV-laser ^{40}Ar/^{39}Ar geochronology of a micaceous mylonite : an example of defect-enhanced argon loss. Contrib Mineral Petrol 142:738-752
Nicolescu S, Reiners PW (2005) (U-Th)/He dating of epidote and andradite garnet. Geochim Cosmochim Acta 69:23
Onstott TC, Phillips D, Pringle-Goodell L (1991) Laser microprobe measurement of chlorine and argon zonation in biotite. Chem Geol 90:145-168
Ouchani S, Dran J-C, Chaumont J (1998) Exfoliation and diffusion following helium ion implantation in fluorapatite: implications for radiochronology and radioactive waste disposal. Appl Geochem 13:707-714
Ozima M (1989) Gases in diamonds. Ann Rev Earth Planet Sci 17:361-384
Ozima M, Podosek FA (2002) Noble Gas Geochemistry. Cambridge University Press.
Parman SW, KelleySP, Ballentine CJ, Van Orman JA (2009) Partitioning and diffusion of noble gases in olivine at mantle pressures. Geochim Cosmochim Acta 73:A995
Parman SW, Kurz MD, Hart SR, Grove TL (2005) Helium solubility in olivine and implications for high ^{3}He /^{4}He in ocean island basalts. Nature 437:1140-1143
Parsons I, Brown WL, Smith JV (1999) ^{40}Ar/^{39}Ar thermochronology using alkali feldspars: real thermal history or mathematical mirage of microtexture? Contrib Mineral Petrol 136:92-110
Phillips D, Onstott TC (1988) Argon isotope zoning in mantle phlogopite. Geology 16:542-546
Pickles CS, Kelley SP, Reddy SM, Wheeler J (1997) Determination of high spatial resolution argon isotope variations in metamorphic biotites. Geochim Cosmochim Acta 61:3809-3833
Porcelli D, Ballentine CJ, Wieler R (eds) (2002) Noble Gases in Geochemistry and Cosmochemistry. Rev Mineral Geochem, Vol. 47. Mineralogical Society of America, Chantilly
Rayleigh (1933) Beryllium and helium. 1. The helium concentration in beryls of different geologic age. Proc R Soc London A 142:370-381
Reddy SM, Kelley SP, Wheeler J (1996) A ^{40}Ar/^{39}Ar laser probe study of micas from the Sesia Zone, Italian Alps: implications for metamorphic and deformation histories. J Metamorph Geol 14:493-508
Reddy SM, Potts GJ, Kelley SP (2001) ^{40}Ar/^{39}Ar ages in deformed potassium feldspar: evidence of microstructural control on Ar isotope systematic. Contrib Mineral Petrol 141:186-200
Reddy SM, Potts GJ, Kelley SP, Arnaud NO (1999) The effects of deformation-induced microstructures on intragrain ^{40}Ar/^{39}Ar ages in potassium feldspar. Geology 27:363-366
Reich M, Ewing RC, Ehlers TA, Becker U (2007) Low-temperature anisotropic diffusion of helium in zircon: implications for zircon (U-Th)/He thermochronometry. Geochim Cosmochim Acta 71:3119-3130
Reiners PW (2009) Nonmonotonic thermal histories and contrasting kinetics of multiple thermochronometers. Geochim Cosmochim Acta 73:3612-3629
Reiners PW, Ehlers TA (eds) (2005) Low Temperature Thermochronology. Rev Mineral Geochem, Vol. 58. Mineralogical Society of America, Chantilly

Reiners PW, Farley KA (1999) Helium diffusion and (U-Th)/He thermochronology of titanite. Geochim Cosmochim Acta 63:3845-3859
Reiners PW, Farley KA, Hickes HJ (2002) He diffusion and (U-Th)/He thermochronometry of zircon: initial results from Fish Canyon Tuff and Gold Butte. Tectonophysics 349:297-308
Reiners PW, Spell TL, Nicolescu S, Zanetti KA (2004) Zircon (U-Th)/He thermochronometry: He diffusion and comparisons with 40Ar/39Ar dating. Geochim Cosmochim Acta 68:1857-1887
Richter FM, Lovera OM, Harrison TM, Copeland P (1991) Tibetan tectonics from $^{40}Ar/^{39}Ar$ analysis of a single Potassium feldspar sample. Earth Planet Sci Lett 105:266-278
Roselieb K, Dersch O, Büttner H, Rauch F (2006) Diffusivity and solubility of He in garnet: An exploratory study using nuclear reaction analysis. Nucl Instruments Meth Phys Res B 244:412-418
Saadoune I, Purton JA, de Leeuw NH (2009) He incorporation and diffusion pathways in pure and defective zircon ZrSiO4: a density functional theory study. Chem Geol 258:182-196
Scaillet S (1996) Excess ^{40}Ar transport scale and mechanism in high pressure phengites: a case study from an eclogitized metabasite of the Dora-Maira nappe, western Alps. Geochim Cosmochim Acta 60:1075-1090
Shukolyokov A, Begemann F (1996) Pu-Xe dating of eucrites. Geochim Cosmochim Acta 60:2453-2471
Shuster DL, Balco G, Cassata WS, Fernandes VA, Garrick-Bethell I, Weiss BP (2010). A record of impacts preserved in the lunar regolith. Earth Planet Sci Lett 290:155-165
Shuster DL, Farley KA (2004) $^{4}He/^{3}He$ thermochronometry. Earth Planet Sci Lett 217:1-17
Shuster DL, Farley KA (2005) Diffusion kinetics of proton-induced ^{21}Ne, ^{3}He, and ^{4}He in quartz. Geochim Cosmochim Acta 69:2349-2359
Shuster DL, Farley KA (2009) The influence of artificial radiation damage and thermal annealing on helium diffusion kinetics in apatite. Geochim Cosmochim Acta 73:183-196
Shuster DL, Farley KA, Sisterton JM, Burnett DS (2004) Quantifying the diffusion kinetics and spatial distributions of radiogenic 4He in minerals containing proton-induced ^{3}He. Earth Planet Sci Lett 217:19-32
Shuster DL, Flowers RM, Farley KA (2006) The influence of natural radiation damage on helium diffusion kinetics in apatite. Earth Planet Sci Lett 249:148-161
Shuster DL, Vasconcelos PM, Heim JA, Farley KA (2005) Weathering geochronology by (U-Th)/He dating of goethite. Geochim Cosmochim Acta 69:659-673
Stockli DF, Farley KA, Walker JD, Blackburn TJ (2005) He diffusion and (U-Th/He) thermochronology of monazite and rutile. Geochim Cosmochim Acta 69:A8
Strutt RJ (1908) Helium and radioactivity in rare and common minerals. Proc R Soc London 80:572-594
Swindle TD (1998) Implications of iodine-xenon studies for the timing and location of secondary alteration. Meteoritics Planet Sci 33:1147-1155
Thomas JB, Cherniak DL, Watson EB (2008) Lattice diffusion and solubility of argon in forsterite, enstatite quartz, and corundum. Chem Geol 253:1-22
Toyota S, Ozima M (1988) Investigation of excess ^{4}He and +Ar in beryl by laser extraction technique. Earth Planet Sci Lett 90:69-76
Trique M, Richon P, Perrier F, Avouac JP, Sabroux JC (1999) Radon emanation and electric potential variations associated with transient deformation near reservoir lakes. Nature 399:137-141
Trull TW, Kurz MD (1993) Experimental measurements of ^{3}He and ^{4}He mobility in olivine and clinopyroxene at magmatic temperatures. Geochim Cosmochim Acta 57:1313-1324
Trull TW, Kurz MD, Jenkins WJ (1991) Diffusion of cosmogenic ^{3}He in olivine and quartz: implications for surface exposure age dating. Earth Planet Sci Lett 103:241-256
Turner G, Busfield A, Crowther SA, Harrison TM, Mojzsis SJ, Gilmour J (2007) Pu-Xe, U-Xe, U-Pb chronology and isotope systematic of ancient zircons from Western Australia. Earth Planet Sci Lett 261:491-499
Villa IM (1994) Multipath Ar transport in Potassium feldspar deduced from isothermal heating experiments. Earth Planet Sci Lett 122:393-401
Villa IM (1996a) Comment on "Age and cooling history of the Manaslu granite: implications for Himalayan tectonics" by Copeland et al. J Volc Geotherm Res 70:255-261
Villa IM (1996b) Reply to the comment on "Multipath Ar transport in K-feldspar deduced from isothermal heating experiments." Earth Planet Sci Lett 140:285-286
Villa IM (2006) From nanometer to megameter: isotopes, atomic-scale processes, and continent-scale tectonic models. Lithos 87:155-173
Villa IM (2010) Disequilibrium textures vs. equilibrium modelling: geochronology at the crossroads. Geol Soc London Spec Pub 332:1-15
Villa IM, Grobety B, Kelley SP, Trigila R, Wieler R (1996) Assessing Ar transport paths and mechanisms for McClure Mountains Hornblende. Contrib Mineral Petrol 126:67-80
Villa IM, Puxeddu M (1994) Geochronology of the Larderello geothermal field - new data and the closure temperature issue. Contrib Mineral Petrol 115:415-426
Villa IM, Ruggieri G, Puxeddu M, Bertini G (2006) Geochronology and isotope transport systematics in a subsurface granite from the Larderello-Travale geothermal system (Italy). J Volc Geoth Res 152:20-50

Warnock AC, Zeitler PK, Wolf RA, Bergman SC (1997) An evaluation of low-temperature apatite U-Th/He thermochronometry. Geochmim Cosmochim Acta 61:5371-5377

Wartho J, Kelley SP, Brooker RA, Carroll MR, Villa IM, Lee MR (1999) Direct measurement of Ar diffusion profiles in a gem-quality Madagascar Potassium feldspar using the ultra-violet laser ablation microprobe (UVLAMP). Earth Planet Sci Lett 170:141-153

Wartho J, Kelley SP, Elphick SC (2005) Estimates of Ar diffusion and solubility in leucite and nepheline: Electron microprobe imaging of Ar distribution in a mineral. Am Mineral 90:954-962

Watson EB, Baxter EF (2007) Frontiers: Diffusion in the Solid Earth. Earth Planet Sci Lett 253:307-327

Watson EB, Cherniak DL (2003) Lattice diffusion of Ar in quartz, with constraints on Ar solubility and evidence of nanopores. Geochim Cosmochim Acta 67:2043-2062

Watson EB, Dohmen R (2010) Non-traditional and emerging methods for characterizing diffusion in minerals and mineral aggregates. Rev Mineral Geochem 72:61-105

Watson EB, Wanser KH, Farley KA (2010b) Anisotropic diffusion in a finite cylinder, with geochemical applications. Geochim Cosmochim Acta 74:614-633

Weber WJ, Ewing RC (2002) Radiation effects in crystalline oxide host phases for the immobilization of actinides. Mat Res Soc Symp Proc 713:443-454

Weins RC, Lal D, Rison W, Wacker JF (1994) Helium isotope diffusion in natural diamonds. Geochim Cosmochim Acta 58:1747-1757

West DP, Lux DR (1993) Dating mylonitic deformation by the ^{40}Ar-^{39}Ar method - an example from the Norumbega fault zone, Maine. Earth Planet Sci Lett 120:221-237

Wolf RA, Farley KA, Silver LT (1996) Helium diffusion and low temperature thermochronometry of apatite. Geochim Cosmochim Acta 60:4231-4240

Zashu S, Hiyagon H (1995) Degassing mechanism of noble gases from carbonado diamonds. Geochim Cosmochim Acta 59:1321-1328

Zeitler PK, Herczig AL, McDougall I, Honda M (1987) U Th-He dating of apatite: a potential thermochronometer. Geochim Cosmochim Acta 51:2865-2868

Zhang XY, Cherniak DJ, Watson EB (2006) Oxygen diffusion in titanite: Lattice diffusion and fast-path diffusion in single crystals. Chem Geol 235:105-123